HHS Public Access

Author manuscript

Nat Neurosci. Author manuscript; available in PMC 2023 February 14.

Published in final edited form as:

Nat Neurosci. 2022 May ; 25(5): 646–658. doi:10.1038/s41593-022-01062-0.

A D2 to D1 shift in dopaminergic inputs to midbrain 5-HT neurons causes anorexia in mice

Xing Cai[1,5,7], **Hailan Liu**[1,7], **Bing Feng**[2], **Meng Yu**[1], **Yang He**[1], **Hesong Liu**[1], **Chen Liang**[1], **Yongjie Yang**[1], **Longlong Tu**[1], **Nan Zhang**[1], **Lina Wang**[1], **Na Yin**[1], **Junying Han**[1], **Zili Yan**[1], **Chunmei Wang**[1], **Pingwen Xu**[1,6], **Qi Wu**[1], **Qingchun Tong**[3], **Yanlin He**[1,2,8], **Yong Xu**[1,4,8]

[1]Children's Nutrition Research Center, Department of Pediatrics, Baylor College of Medicine, Houston, TX, USA.

[2]Brain Glycemic and Metabolism Control Department, Pennington Biomedical Research Center, Louisiana State University, Baton Rouge, LA, USA.

[3]Brown Foundation Institute of Molecular Medicine, University of Texas Health Science Center at Houston, Houston, TX, USA.

[4]Department of Molecular and Cellular Biology, Baylor College of Medicine, Houston, TX, USA.

[5]Present address: Kunming Institute of Zoology, Chinese Academy of Sciences, Kunming, Yunnan, China.

[6]Present address: Division of Endocrinology, Department of Medicine, University of Illinois at Chicago, Chicago, IL, USA.

[7]These authors contributed equally: Xing Cai, Hailan Liu.

[8]These authors jointly supervised this work: Yanlin He, Yong Xu.

Abstract

Midbrain dopamine (DA) and serotonin (5-HT) neurons regulate motivated behaviors, including feeding, but less is known about how these circuits may interact. In this study, we found that DA neurons in the mouse ventral tegmental area bidirectionally regulate the activity of 5-HT neurons in the dorsal raphe nucleus (DRN), with weaker stimulation causing DRD2-dependent inhibition

yanlin.he@pbrc.edu; yongx@bcm.edu.

Author contributions

X.C., H.L. and Yanlin He were involved in experimental design, in most of the procedures, data acquisition and analyses and in writing the manuscript. P.X., H.L., B.F. and C.W. assisted in some of the histology and electrophysiology studies. M.Y., Yang He, H.L., C.L., Y.Y., L.T., N.Z., L.W., N.Y., J.H. and Z.Y. assisted in surgical procedures and in production of study mice. Q.W. and Q.T. were involved in study design and in writing the manuscript. Yanlin He and Y.X. are the guarantors of this work and, as such, had full access to all the data in the study and take responsibility for the integrity of the data and the accuracy of the data analysis.

Competing interests

The authors declare no competing interests.

Extended data is available for this paper at https://doi.org/10.1038/s41593-022-01062-0.

Supplementary information The online version contains supplementary material available at https://doi.org/10.1038/s41593-022-01062-0.

Peer review information *Nature Neuroscience* thanks Roger Adan, Mitsuko Watabe-Uchida and the other, anonymous, reviewer(s) for their contribution to the peer review of this work.

and overeating, while stronger stimulation causing DRD1-dependent activation and anorexia. Furthermore, in the activity-based anorexia (ABA) paradigm, which is a mouse model mimicking some clinical features of human anorexia nervosa (AN), we observed a DRD2 to DRD1 shift of DA neurotransmission on 5-HT^{DRN} neurons, which causes constant activation of these neurons and contributes to AN-like behaviors. Finally, we found that systemic administration of a DRD1 antagonist can prevent anorexia and weight loss in ABA. Our results revealed regulation of feeding behavior by stimulation strength-dependent interactions between DA and 5-HT neurons, which may contribute to the pathophysiology of AN.

AN is an eating disorder characterized by self-starvation, hyperactivity and excessive weight loss and has the highest mortality rate among all psychiatric diseases[1]. There are no approved treatments for AN, and the underlying pathophysiology is unclear.

A recent genome-wide association study (GWAS) analyzed the association between 149 cell types and genetic variants in 16,992 patients with AN and found that DA neurons and 5-HT neurons are among the top-ranked cell types associated with human AN, although these associations did not reach significance[2]. DA neurons in the ventral tegmental area (VTA) regulate motivated behaviors, including feeding and physical activity[3,4]. Interestingly, DA^{VTA} neurons exhibit bimodal firing patterns[5]. Tonically, DA^{VTA} neurons fire at low frequencies (1–8 Hz), resulting in low levels of DA release that primarily activates high-affinity D2 dopamine receptor (DRD2), a Gαi-coupled inhibitory receptor. On the other hand, DA^{VTA} neurons can also display phasic bursting at high frequencies (>10 Hz), leading to transient high-level DA surges that activate low-affinity D1 dopamine receptor (DRD1), a Gαs-coupled excitatory receptor[6]. Interestingly, multiple polymorphisms in the gene encoding DRD2 are associated with AN[7–12], although the GWASs did not confirm this. In addition, patients with AN express higher levels of dopamine transporter (DAT)[10]. Restricting-type patients with AN show increased eye blinking responses, a suggestive indicator of increased DA activity[13], whereas patients who recovered from AN have lower DA metabolites in the cerebrospinal fluid[14]. Although these association studies suggest that DA dysfunction could contribute to the development and/or persistence of AN, the causal relation has not been validated.

The brain 5-HT is primarily synthesized by neurons in the dorsal raphe nucleus (DRN)[15]. These 5-HT^{DRN} neurons play essential roles in the regulation of feeding[16]. 5-HT analogs —for example, d-fenfluramine[17] and lorcaserin[18]—induce potent anorexia in rodents and humans. Conversely, compounds that suppress central 5-HT signals produce hyperphagia and weight gain in humans and rodents[19]. Furthermore, patients with AN have elevated 5-HT metabolites in their cerebrospinal fluid, suggesting increased 5-HT bioavailability in the brain[20]. In addition, many brain imaging studies have demonstrated increased 5-HT receptor binding[21–23] and 5-HT transporter activity[24] in patients with AN.

Although dysfunctions of DA and 5-HT neurons have been associated with human AN, how these two neural populations contribute to AN phenotypes remains unclear. In this study, we first demonstrated that DA^{VTA} neurons project to the DRN and regulate activity of 5-HT^{DRN} neurons in a strength-dependent manner. We then examined effects of the DA^{VTA}→DRN circuit, when optogenetically activated at various frequencies, on feeding behavior in

animals and explored the role of DRD1 and DRD2 in mediating these effects. Furthermore, we combined a widely used rodent model for AN and a battery of fiber photometry, chemogenetics and Cre-loxP knockout mouse models to determine the relevance of the DA^{VTA}→DRN circuit, including DRD1 and DRD2 actions, in the regulation of AN-like behaviors. Finally, we tested potential therapeutic effects of a DRD1 antagonist on anorexia and weight loss in mice.

Results

A strength-dependent effect of DA on 5-HT^{DRN} neurons.

It has been reported that 5-HT^{DRN} neurons receive innervations from a small portion of DA^{VTA} neurons[25–28]. We further found that both DRD1 and DRD2 mRNAs are co-expressed by a portion of 5-HT^{DRN} neurons (Extended Data Fig. 1a–c). Using slice electrophysiology recordings in the presence of cocktail blockers (30 μM D-AP5, 30 μM CNQX and 50 μM bicuculline), we found that low concentrations of DA (0.01–0.2 μM) significantly decreased firing frequency and hyperpolarized resting membrane potential in 5-HT^{DRN} neurons (tdTOMATO-labeled DRN neurons in *TPH2-CreER/Rosa26-LSL-tdTOMATO* mice); strikingly, high concentrations of DA (0.8 μM, 1 μM and 10 μM) significantly activated 5-HT^{DRN} neurons (Fig. 1a). No significant effect was induced by an extremely low concentration (0.001 μM) of DA treatment, whereas intermediate concentrations (0.4 μM and 0.6 μM) only altered firing frequency or resting membrane potential (Fig. 1a). We further found that the inhibition induced by 0.05 μM DA was not affected by pre-incubation with SCH23390, a DRD1 antagonist; however, eticlopride, a DRD2 antagonist, abolished the inhibition (Fig. 1b). On the other hand, the activation induced by 10 μM DA was not affected by eticlopride but was significantly attenuated by SCH23390 (Fig. 1c). Consistent with previous reports[6], our results indicate that low concentrations of DA inhibit 5-HT^{DRN} neurons via DRD2, whereas high concentrations of DA act primarily upon DRD1 to activate these neurons.

To further examine the neurotransmission between DA^{VTA} and 5-HT^{DRN} neurons, we bred to generate compound *TPH2-CreER/DAT-CreER/Rosa26-LSL-tdTOMATO* mice. Note that, in *DAT-CreER/Rosa26-LSL-tdTOMATO* mice, a tamoxifen injection induced Cre activity only in the VTA and substantia nigra (SN) but not in the DRN (Extended Data Fig. 2a), although the DRN is known to harbor DAT-expressing neurons[29]. Similarly, in *TPH2-CreER/Rosa26-LSL-tdTOMATO* mice, a tamoxifen injection induced Cre activity only in the DRN but not in the VTA and SN (Extended Data Fig. 2b). We then stereotaxically injected Cre-dependent AAV-expressing ChR2-EYFP into the VTA of compound *TPH2-CreER/DAT-CreER/Rosa26-LSL-tdTOMATO* mice to express ChR2 specifically in DA^{VTA} neurons and their fibers/terminals. The same mice also received stereotaxic injections of Ad-iN/WED, an anterograde trans-synaptic viral tracer[30], into the VTA. Ad-iN/WED expressed green fluorescent protein (GFP)-tagged wheat germ agglutinin (WGA-GFP) in a Cre-dependent manner; WGA-GFP is an anterograde trans-synaptic tracer, which can label the somas of downstream neurons[30], although it can also travel retrogradely[31]. WGA-labeled somas in the DRN were, therefore, identified as putative downstream neurons of DA^{VTA} neurons. Note that these mice also express tdTOMATO in 5-HT^{DRN} neurons due

to the combination of *TPH2-CreER* and *Rosa26-LSL-tdTOMATO* alleles. Thus, we used slice electrophysiology to record $WGA^{+}tdTOMATO^{+}$ neurons in the DRN in response to photostimulation of ChR2-expressing DA^{VTA} fiber/terminals (Fig. 1d). We found that blue pulses at 2 Hz caused a significant inhibition in $5\text{-}HT^{DRN}$ neurons (Fig. 1e,f). Interestingly, blue pulses at 5 Hz failed to significantly alter the resting membrane potential, although it can still reduce the firing frequency (Fig. 1f). Strikingly, blue pulses at 10 Hz, 20 Hz and 30 Hz led to activation in $5\text{-}HT^{DRN}$ neurons (Fig. 1e,f). The 2-Hz-induced inhibition was not affected by pre-incubation with SCH23390 (the DRD1 antagonist) but was abolished by eticlopride (the DRD2 antagonist) (Fig. 1g,h). On the other hand, 20-Hz-induced activation was not affected by eticlopride (Fig. 1i,j). Interestingly, in the presence of SCH23390, 20-Hz blue light pulses did not alter the firing frequency but still modestly depolarized $5\text{-}HT^{DRN}$ neurons, although this depolarization was significantly attenuated compared to that in the absence of SCH23390 (Fig. 1i,j). These results revealed interesting bidirectional regulatory effects of DA^{VTA} neurons on $5\text{-}HT^{DRN}$ neurons. Thus, low-frequency stimulation (2 Hz) of DA^{VTA} neurons inhibits $5\text{-}HT^{DRN}$ neurons via DRD2-mediated mechanisms, whereas high-frequency stimulation (10–30 Hz) of DA^{VTA} neurons activates $5\text{-}HT^{DRN}$ neurons via DRD1-mediated mechanisms.

Bidirectional effects of the DA^{VTA}→DRN circuit on feeding.

We stereotaxically injected Cre-dependent AAV-expressing ChR2-EYFP into the VTA of *DAT-CreER* mice to express ChR2 specifically in DA^{VTA} neurons and their fibers/terminals (Extended Data Fig. 3a,b). These mice were also implanted with an optic fiber to target the DRN, which allowed us to examine effects of the DA^{VTA}→DRN circuit on refeeding behavior (Fig. 2a and Extended Data Fig. 3c). We found that 2-Hz blue light pulses significantly increased refeeding in hungry mice compared to the same mice receiving 2-Hz yellow light pulses (Fig. 2b). On the other hand, 20-Hz blue light pulses shed onto the DRN resulted in a significant suppression on food intake (Fig. 2c). We then tested a sequential protocol with three repeated 5-minute blocks of blue light stimulation separated by three blocks of 5-minute light-off. In this protocol, 2-Hz blue light pulses did not significantly alter food intake in each 5-minute block but significantly increased the total food intake during the entire 15-minute light-on period (Extended Data Fig. 3d). Interestingly, 20-Hz blue light pulses significantly decreased food intake in two out of three 5-minute blocks as well as the total food intake during the entire 15-minute light-on period (Extended Data Fig. 3e). We also examined an intermediate frequency (5 Hz) and found no significant changes in food intake (Extended Data Fig. 3f). Notably, pre-injections of 100 ng of eticlopride (the DRD2 inhibitor) into the DRN abolished the increased feeding induced by 2-Hz photostimulation (Fig. 2d). Similarly, pre-injections of 10 ng of SCH23390 (the DRD1 inhibitor) into the DRN abolished the suppression of feeding induced by 20-Hz photostimulation (Fig. 2e). Thus, these results suggest that low-frequency stimulation of the DA^{VTA}→DRN circuit increases food intake via DRD2 actions in the DRN, whereas high-frequency stimulation of the same circuit decreases food intake via DRD1 actions in the DRN. We then stereotaxically injected the Cre-dependent AAV-expressing ChR2 into the VTA and the Cre-dependent AAV-expressing hM4Di into the DRN in compound *DAT-CreER/TPH2-CreER* mice to express ChR2 in DA^{VTA} neurons and hM4Di in $5\text{-}HT^{DRN}$ neurons. An optic fiber was implanted to target the DRN to allow photostimulation of the

DA^{VTA}→DRN projections (Extended Data Fig. 3g). After a saline intraperitoneal injection, 20-Hz blue light pulses shed to the DRN significantly reduced food intake; however, after a clozapine *N*-oxide (CNO) injection, which inhibited 5-HT^{DRN} neurons, the same 20-Hz blue light pulses had no effect on food intake (Extended Data Fig. 3h). These results further supported the model that high-frequency stimulation of the DA^{VTA}→DRN projections inhibits food intake via activation of 5-HT^{DRN} neurons.

We examined the valence associated with DA^{VTA}→DRN photostimulation using a real-time place preference test. We found that, in hungry mice, 2-Hz photostimulation of the DA^{VTA}→DRN projections transmitted no clear valence, whereas 20-Hz photostimulation transmitted a strong positive valence (Fig. 2f). Interestingly, when one side of the place preference apparatus contained food pellets, hungry mice showed a clear preference to the food-containing side, which was completely neutralized by 20-Hz photostimulation associated with the other side, accompanied by decreased food intake (Fig. 2g and Extended Data Fig. 3i), but 2-Hz photostimulation had no effect (Fig. 2g). Thus, these results indicate that high-frequency stimulation of the DA^{VTA}→DRN circuit transmits a strong positive valence that can compete against hungry animals' desire for food.

Because DA^{VTA} neurons are known to send strong projections to the nucleus of accumbens (NAc)[32], we also examined effects of the DA^{VTA}→NAc circuit on feeding and valence (Extended Data Fig. 3j). No significant changes in food intake were observed when the DA^{VTA}→NAc circuit was photostimulated at 2 Hz, 5 Hz or 20 Hz (Extended Data Fig. 3k). Surprisingly, in hungry mice, both 2-Hz and 20-Hz photostimulation of the DA^{VTA}→NAc projections failed to transmit a clear valence and had no effect on animals' preference to the food-containing side (Extended Data Fig. 3l,m). However, in satiated mice, both 2-Hz and 20-Hz photostimulation of the same circuit resulted in a positive valance (Extended Data Fig. 3n), indicating that the valence signals associated with the DA^{VTA}→NAc circuit are influenced by the nutritional state of animals.

DRN-projecting DA^{VTA} neurons mediate activity-based anorexia.

Here, we stereotaxically injected a retrograde Cre-dependent HSV vector into the DRN of *DAT-CreER* mice to express GCaMP6 (an intracellular calcium sensor) specifically in DA^{VTA} neurons that project to the DRN (Fig. 3a and Extended Data Fig. 4a). These mice were also implanted with a photodetector to target the VTA, which allowed us to monitor the intracellular calcium in the subset of DRN-projecting DA^{VTA} neurons in freely moving mice. We first subjected naive mice to a 24-hour fasting followed by refeeding. Interestingly, the GCaMP6 signals in DRN-projecting DA^{VTA} neurons displayed robust dynamics at different nutritional states on a time scale of minutes. In particular, compared to the fed state, DRN-projecting DA^{VTA} neurons in fasted mice showed significantly elevated GCaMP6 signals, which were reduced by 60-minute refeeding (Fig. 3b). Then, these mice were exposed to the ABA paradigm, a widely used rodent model to mimic clinical features of AN[33], which is comprised of ad libitum access to running wheels and a restricted feeding schedule (Methods). Strikingly, in ABA mice, the GCaMP6 signals in DRN-projecting DA^{VTA} neurons maintained at significantly higher levels than in naive mice, and 60-minute refeeding did not affect the signals (Fig. 3b). Notably, during these studies, we also observed

rapid elevations in the GCaMP6 signals in DRN-projecting DA^{VTA} neurons that were tightly associated with the onset of each eating bout and lasted for only a few seconds (Extended Data Fig. 4b). Interestingly, these bout-associated transients were not significantly altered in ABA mice (Extended Data Fig. 4b,c).

We then stereotaxically injected a retrograde tracer, Green RetroBeads, into the DRN of *DAT-CreER/Rosa26-LSL-tdTOMATO* mice and used slice electrophysiology to record the firing activity of DRN-projecting DA^{VTA} neurons (labeled by both tdTOMATO and Green RetroBeads; Fig. 3c and Extended Data Fig. 4d). We first analyzed the tonic firing of these DRN-projecting DA^{VTA} neurons and found that firing frequency and resting membrane potential were both significantly increased in ABA mice compared to fasted naive mice (Fig. 3d). Furthermore, we compared the phasic bursting of these neurons and noted that DRN-projecting DA^{VTA} neurons in ABA mice showed significantly higher bursting event frequency and bursting score (Fig. 3e,f).

Furthermore, we stereotaxically injected an AAV-hSyn-GRAB_DA1h into the DRN of wild-type mice to express the DA biosensor (Fig. 3g). These mice were also implanted with a photodetector to target the DRN, which allowed us to monitor the DA levels. In naive mice, we observed that fasting induced a modest but significant increase in DA levels compared to the ad libitum condition (Fig. 3h). Interestingly, DA levels in the DRN were negatively correlated with the amount of food intake (Extended Data Fig. 4e). However, after these mice were subjected to the ABA paradigm, DA levels in the DRN were significantly elevated compared to naive mice and did not show the refeeding-induced reduction (Fig. 3h). We also observed short-lived (<10-second) elevations in DA levels in the DRN that were tightly associated with the onset of each eating bout—responses that were similar between naive and ABA mice (Extended Data Fig. 4f,g).

Because the DRN-projecting DA^{VTA} neurons were constantly activated during the ABA period, we sought to examine whether chemogenetic inhibition of these neurons could alleviate the ABA phenotypes. To this end, we stereotaxically injected a retrograde Cre-dependent AAV vector into the DRN of *DAT-CreER* mice to express hM4Di specifically in the DRN-projecting DA^{VTA} neurons, which allowed us to use CNO injections to selectively inhibit the DA^{VTA}→DRN circuit (Fig. 3i and Extended Data Fig. 5a–e). When subjected to the ABA paradigm, these mice with CNO injections showed attenuated body weight loss and significantly improved survival rate (Fig. 3j,k and Extended Data Fig. 5f). Notably, the chemogenetic inhibition of the DA^{VTA}→DRN circuit significantly increased food intake (Fig. 3l) and trended to decrease running wheel activity (Fig. 3m). Collectively, these results indicate that selective inhibition of DRN-projecting DA^{VTA} neurons can at least partially rescue anorexia and hyperactivity in ABA mice, resulting in a significantly better survival, although these results could not fully exclude the potential involvement of NAc collaterals from these DRN-projecting DA^{VTA} neurons.

5-HT^{DRN} neurons mediate activity-based anorexia.

Because DA^{VTA} neurons have bidirectional regulations on 5-HT^{DRN} neurons, we further explored the physiological relevance of 5-HT^{DRN} neurons in the ABA phenotypes. Here, we stereotaxically injected a Cre-dependent AAV vector expressing GCaMP6 and implanted a

photodetector to target the DRN of *TPH2-CreER* mice, to monitor the GCaMP6 signals in 5-HT^{DRN} neurons (Fig. 4a). We found that, in naive mice, the 24-hour fasting significantly decreased the GCaMP6 signals in 5-HT^{DRN} neurons, which were restored by refeeding (Fig. 4b). Strikingly, in ABA mice, the GCaMP6 signals in 5-HT^{DRN} neurons maintained at significantly higher levels than in naive mice, and refeeding did not affect the signals (Fig. 4b). Consistently, using the slice electrophysiology, we demonstrated that 5-HT^{DRN} neurons in ABA mice showed significantly higher firing frequency and resting membrane potential than those from naive fasted mice (Fig. 4c).

We stereotaxically injected a Cre-dependent AAV vector into the DRN of *TPH2-CreER* mice to express hM4Di specifically in 5-HT^{DRN} neurons, which allowed us to use CNO injections to selectively inhibit 5-HT^{DRN} neurons (Fig. 4d and Extended Data Fig. 6a–c). Chemogenetic inhibition of 5-HT^{DRN} neurons in ABA mice significantly increased food intake, associated with tendencies of decreased running wheel activity, attenuated body weight loss and better survival rate (Fig. 4e–h and Extended Data Fig. 6d). Collectively, these results indicate that selective inhibition of 5-HT^{DRN} neurons can at least partially rescue anorexia and hyperactivity in ABA mice.

We further examined whether 5-HT synthesis in the DRN is required to mediate the ABA phenotypes. To this end, we stereotaxically injected AAV-Cre-GFP or AAV-GFP into the DRN midline of *TPH2$^{fl/fl}$* mice to generate mice with reduced TPH2 expression in the DRN (TPH2^{DRN}-KO) and controls (Fig. 4i and Extended Data Fig. 6e). Compared to controls, TPH2^{DRN}-KO mice showed significantly increased food intake and reduced running wheel activity, which was associated with significantly attenuated body weight loss and better survival rate (Fig. 4j–m and Extended Data Fig. 6e–g). These results indicate that blockade of 5-HT synthesis in the DRN can prevent anorexia and hyperactivity in ABA mice.

DRD1 in 5-HT^{DRN} neurons mediates activity-based anorexia.

We sought to determine whether DRD1 actions in the DRN contribute to the development of the ABA phenotypes. To this end, we generated mice lacking DRD1 selectively in the DRN (DRD1^{DRN}-KO) by stereotaxically delivering AAV-Cre-GFP into the DRN of *Drd1$^{fl/fl}$* mice. Compared to control mice, loss of DRD1 in the DRN attenuated ABA-induced weight loss and significantly improved survival rate, increased food intake and reduced running wheel activity (Fig. 5a–d). Notably, DRD1^{DRN}-KO mice showed a significantly higher baseline body weight compared to control mice (Extended Data Fig. 7a). Although this phenotype further supports the weight-reducing effects of DRD1 in the DRN, the different baseline body weight may have confounded the ABA phenotypes in these mice. To cope with this potential issue, we generated and validated mice lacking DRD1 only in 5-HT neurons (DRD1^{TPH2}-KO), which showed similar baseline body weight as their control littermates (Extended Data Fig. 7b–d). When subjected to the ABA paradigm, DRD1^{TPH2}-KO mice showed less body weight loss and significantly improved survival rate compared to control littermates, which was associated with significantly increased food intake and attenuated running wheel activity during the ABA period (Fig. 5e–h). Collectively, these results indicate that loss of DRD1 in 5-HT^{DRN} neurons can partially rescue anorexia and hyperactivity in ABA mice. Given the role of DRD1 in ABA phenotypes, we further

examined effects of *Drd1* deletion on 5-HT^{DRN} neuron activity using fiber photometry. At the naive condition, mice lacking DRD1 in 5-HT neurons showed similar responses to various feeding conditions as control mice (Fig. 5i). Interestingly, during the ABA period, DRD1 deletion significantly reduced 5-HT^{DRN} neuron activity compared to control mice (Fig. 5j).

Because anorexia and weight loss can be ameliorated by *Drd1* deletion, we sought to examine whether pharmacological inhibition of DRD1 can prevent AN-like phenotypes in ABA mice. Daily intraperitoneal injections of SCH23390 (the DRD1 antagonist) during the ABA period attenuated weight loss and significantly improved survival rate (Fig. 5k,l and Extended Data Fig. 7e). Notably, SCH23390 significantly increased food intake and attenuated running wheel activity (Fig. 5m,n). These results indicate that systemic administration of the DRD1 antagonist can at least partially ameliorate AN-like behaviors in ABA mice.

DRD2 in 5-HT^{DRN} neurons prevents anorexia.

We generated mice lacking DRD2 selectively in the DRN (DRD2^{DRN}-KO) by stereotaxically delivering AAV-Cre-GFP into the DRN of *Drd2*$^{fl/fl}$ mice. However, when DRD2^{DRN}-KO mice were subjected to the ABA paradigm, they displayed similar body weight loss, survival rate, food intake and running wheel activity as control mice (*Drd2*$^{fl/fl}$ mice receiving AAV-GFP injected in the DRN; Fig. 6a–d and Extended Data Fig. 8a). We then generated mice lacking DRD2 in 5-HT neurons (DRD2^{TPH2}-KO; Extended Data Fig. 8b–d). When subjected to the ABA paradigm, DRD2^{TPH2}-KO mice showed similar body weight loss, survival rate, food intake and running wheel activity as control littermates (Fig. 6e–h). Thus, loss of DRD2 in 5-HT^{DRN} neurons does not produce additive effects to worsen anorexia in mice subjected to the ABA paradigm.

Interestingly, when mice were exposed to the running wheels and fed ad libitum, we noted that DRD2^{TPH2}-KO mice displayed significant weight loss, whereas control mice did not significantly lose weight (Fig. 6i). In addition, DRD2^{TPH2}-KO mice showed modest reductions in food intake compared to controls, although running wheel activity was not different (Fig. 6j,k). Thus, these results indicate that loss of DRD2 in 5-HT neurons renders animals' increased susceptibility to anorexia and weight loss in the context of hyperactivity.

Discussion

In this study, we found that low-frequency (2-Hz) stimulation of DA^{VTA} neurons inhibits 5-HT^{DRN} neurons via DRD2, whereas high-frequency (10–30-Hz) stimulation of DA^{VTA} neurons activates 5-HT^{DRN} neurons via DRD1. The DA^{VTA}→DRN circuit promotes or suppresses feeding behavior in a frequency-dependent manner through either DRD2 or DRD1 actions (Fig. 6l). Furthermore, the ABA in mice is associated with constantly elevated activity of both DRN-projecting DA^{VTA} neurons and 5-HT^{DRN} neurons, and chemogenetic inhibition of these neurons can partially rescue the AN-like phenotypes. Finally, we demonstrated that deletion of DRD1 in 5-HT neurons or a DRD1 antagonist can ameliorate AN-like phenotypes, whereas loss of DRD2 in 5-HT neurons makes mice more prone to anorexia and weight loss during hyperactivity.

Despite the well-established roles of 5-HT^{DRN} neurons and their downstream circuits in the regulation of food intake[16], little is known about the upstream neural networks that regulate 5-HT^{DRN} neuron activity in the context of feeding control. Early circuitry mapping efforts demonstrated that a small portion of DA^{VTA} neurons innervate 5-HT^{DRN} neurons[25–28]. Consistently, here, we further provide functional evidence that DRD2-mediated tonic inhibition on 5-HT^{DRN} neurons shifts to DRD1-mediated excitation when DA^{VTA} neurons transit from tonic firing to phasic bursting. Using the optogenetic approach to manipulate the DA^{VTA}→DRN circuit at a tonic firing frequency (2 Hz) or at a bursting frequency (20 Hz), we further demonstrated that these two firing patterns evoked completely opposite effects on feeding behaviors in mice. In particular, 2 Hz promotes feeding via DRD2 in the DRN, but 20 Hz suppresses feeding via DRD1. Notably, 20-Hz stimulation of the DA^{VTA}→DRN circuit also transmits a strong positive valence that can compete against hungry animals' desire for food. Collectively, these data identified DA^{VTA} neurons as one upstream regulator of 5-HT^{DRN} neurons in the context of feeding control. Notably, 5-HT^{DRN} neurons partially overlap with glutamatergic neurons within the DRN[34]. Recent evidence indicates that glutamatergic neurons in the DRN inhibit feeding, whereas GABAergic neurons in the DRN promote feeding by inhibiting the adjacent glutamatergic neurons[35]. Thus, a subset of glutamatergic 5-HT^{DRN} neurons may also receive inhibitory inputs from local GABA^{DRN} neurons to regulate food intake. Whether DA^{VTA} neurons can indirectly regulate glutamatergic 5-HT^{DRN} neurons via these GABA^{DRN} neurons warrants further investigation. In addition, GABAergic neurons in the VTA also send monosynaptic projections to 5-HT^{DRN} neurons[27], but the functional relevance of this GABAergic VTA→DRN circuit in feeding control remains unclear.

Given the bidirectional regulations of the DA^{VTA}→DRN circuit on feeding behavior, we further explored the functional relevance of this circuit in the ABA paradigm, which is comprised of unlimited access to running wheels and a restricted feeding schedule. Under these conditions, rodents and other mammals rapidly develop 'self-starvation' and weight loss, compared to animals subjected to either running wheels or restricted feeding alone[36]. Although the ABA paradigm does not fully recapitulate AN in humans, it resembles many AN phenotypes seen in patients, including hyperactivity, hypothermia, activated hypothalamus–pituitary–adrenal axis, stomach ulcers, bone loss, endocrine dysregulations and, ultimately, death[33]. Notably, female rodents are more prone to ABA phenotypes than males[37], resembling the high prevalence of AN in women[38]. Here, we found that DRN-projecting DA^{VTA} neurons in ABA mice show constantly elevated activities and enhanced bursting. Consistently, ABA mice have constantly elevated DA levels in the DRN, associated with elevated 5-HT^{DRN} neural activities. Chemogenetic inhibition of either DRN-projecting DA^{VTA} neurons or 5-HT^{DRN} neurons, or disruption of TPH2 (the rate-limiting enzyme for 5-HT synthesis), partially alleviates the ABA phenotypes, supporting the notion that the elevated activity of the DA^{VTA}→DRN circuit contributes to AN-like behaviors in ABA mice. Considering that DA neurons and 5-HT neurons are among the top-ranked cell types associated with human AN[2], these results suggest that the abnormal activity of the DA^{VTA}→DRN circuit underlie the pathophysiology of AN in at least a subset of patients.

It is worth mentioning that, in naive mice, feeding conditions regulate activities of DRN-projecting DA^{VTA} neurons and 5-HT^{DRN} neurons in an exactly opposite fashion.

In particular, DRN-projecting DA^{VTA} neurons are activated by fasting and inhibited by refeeding, whereas 5-HT^{DRN} neurons are inhibited by fasting and activated by refeeding. The opposite dynamics suggest that, in naive mice, DRD2 predominantly mediates an inhibitory neurotransmission from DA^{VTA} neurons to 5-HT^{DRN} neurons. On the other hand, when mice develop the ABA phenotypes, DRN-projecting DA^{VTA} neurons show increased bursting firing, which is known to produce a large phasic DA release that mainly activates DRD1 (ref. [39]). Consistently, in vivo fiber photometry demonstrated that, in ABA mice, activities of both DRN-projecting DA^{VTA} neurons and 5-HT^{DRN} neurons are constantly elevated and no longer respond to various feeding conditions, and genetic deletion of DRD1 from 5-HT neurons substantially reduces their neural activity, suggesting a predominant DRD1-mediated excitatory neurotransmission on 5-HT^{DRN} neurons. Given the anorexigenic nature of 5-HT^{DRN} neurons, the reduced activity of these neurons presumably accounts for enhanced feeding and survival in ABA mice with *Drd1* deletion. On the other hand, loss of DRD2, either in the DRN or in 5-HT neurons, has no detectable effect in ABA mice, in line with an already reduced DRD2-mediated neurotransmission onto 5-HT^{DRN} neurons at the ABA condition. Thus, we suggest that a DRD2→DRD1 shift of DA neurotransmission on 5-HT^{DRN} neurons occurs during the development of ABA, which causes a constant activation of 5-HT^{DRN} neurons and contributes, at least partially, to AN-like behaviors. Similarly, shifts between DRD1-mediated and DRD2-mediated neurotransmissions, or shifts between phasic bursting and tonic firing of DA neurons, have been implicated to differently regulate behavioral conditioning[3], averse response to nicotine withdrawal[40] and depression-like behavior during social defeat[41].

No US Food and Drug Administration-approved pharmacological treatments are currently available for patients with AN. Our results suggest that either DRD2 activation or DRD1 inhibition might produce therapeutic benefits. Supporting a role of DRD2 agonism, aripiprazole, an atypical antipsychotic medicine that activates DRD2, was found to promote weight gain in patients with AN[42]. Intriguingly, several clinical studies indicate that olanzapine, another atypical antipsychotic medicine that blocks DRD2, can also promote body weight gain in patients with AN[43]. It is worth mentioning that both aripiprazole and olanzapine also have complex actions on multiple receptors for 5-HT and/or histamine, which may also account for the clinical outcome. Nevertheless, systemic administration of eticlopride (the DRD2 antagonist) was reported to ameliorate the ABA phenotypes in mice[44]. Because abundant DRD2 is expressed pre-synaptically by DA neurons as an inhibitory autoreceptor to reduce DA neuron firing, DA synthesis and DA release[45], DRD2 agonists and antagonists may alter endogenous DA bioavailability throughout the brain via the pre-synaptic autoreceptor and result in complex outcomes. In addition, patients with AN who carry DRD2 polymorphisms[7–12] may not respond well to DRD2 medicines. On the other hand, we found that SCH23390 (the DRD1 antagonist), when systemically administrated, can partially prevent anorexia and weight loss in ABA mice. Consistently, SCH23390 was also reported to substantially reduce anorexia and hyperactivity in animals exposed to amphetamine[46]. Although there are no clinical data regarding effects of DRD1 antagonists in patients with AN, our preclinical evidence indicates that DRD1 antagonism may be a better therapeutic strategy for at least subsets of patients with AN.

It is important to point out that effects of the brain DA system on feeding are complex. For example, mice born without DA synthesis are hypoactive, apathetic and aphagic, phenotypes that can be rescued by supplement with a DA analog[4,47]. Similarly, anorexia induced by repeated restraint stress is associated with decreased DA^{VTA} neuron activity[48]. However, chemogenetic activation of DA^{VTA} neurons increases meal frequency but reduces meal size, resulting in unaffected total food intake[49]. Interestingly, activation of DA^{VTA} neurons can inhibit binge-like eating, a feeding behavior in satiated animals driven by hedonic values of high palatable food[18]. Furthermore, chemogenetic stimulation of DRD1-expressing neurons in the lateral parabrachial nucleus inhibits refeeding in hungry mice, whereas inhibition of these neurons promotes refeeding[50]. On the other hand, chemogenetic activation of DRD1-expressing neurons in the NAc increases food intake, whereas stimulation of NAc DRD2-expressing neurons decreases food intake in satiated, unfasted mice[51]. Furthermore, overexpression of DRD2 in the NAc worsens the anorexia in female ABA mice[52]. In addition, the optogenetic stimulation of DRD1-expressing neurons in the medial prefrontal cortex promotes feeding in unfasted mice[53]. Thus, effects of the brain DA system on feeding and AN-like phenotypes appear to be highly heterogeneous and can be influenced by the brain regions, the DA receptors and the nutritional and psychological states of animals. Our findings further add to this complexity as activations of DA^{VTA} neurons at different strengths (weak tonic firing versus strong phasic bursting) could result in completely opposite effects on feeding.

In summary, recent human genetic efforts revealed various genetic variants associated with AN[2]. Taking advantage of these resources, we focused, in this study, on the brain DA and 5-HT circuits and provided evidence that activated DRN-projecting DA^{VTA} neurons and a DRD2→DRD1 shift of DA neurotransmission on $5\text{-}HT^{DRN}$ neurons can trigger AN-like behaviors. These findings provide a mechanistic framework for developing novel therapeutic strategies for this devastating and life-threatening disease.

Online content

Any methods, additional references, Nature Research reporting summaries, source data, extended data, supplementary information, acknowledgements, peer review information; details of author contributions and competing interests; and statements of data and code availability are available at https://doi.org/10.1038/s41593-022-01062-0.

Methods

Mice.

Multiple lines of transgenic mice were used in the current study, as summarized in Supplementary Table 1. *TPH2-CreER* mice were purchased from Jackson Laboratory (016584) that express tamoxifen-inducible Cre recombinase selectively in 5-HT neurons, as we validated previously[54]. *DAT-CreER* mice were purchased from Jackson Laboratory (016583) that express tamoxifen-inducible Cre recombinase selectively in DA neurons, as we validated previously[54]. For electrophysiological studies, we crossed *Rosa26-LSL-tdTOMATO* allele (Jackson Laboratory, 007905)[55] onto *DAT-CreER* or *TPH2-CreER* to generate *DAT-CreER/ Rosa26-LSL-tdTOMATO* mice or *TPH2-CreER/Rosa26-LSL-*

tdTOMATO mice. Tamoxifen inductions (0.2 mg g^{-1}, intraperitoneal; Supplementary Table 1) induced tdTOMATO expression selectively in DA and 5-HT neurons, respectively. We also crossed to generate compound *TPH2-CreER/DAT-CreER/Rosa26-LSL-tdTOMATO* mice for optogenetic/chemogenetic studies and slice electrophysiology studies, as described below. For other in vivo experiments, we crossed *C57Bl6j* mice (purchased from the mouse facility of Baylor College of Medicine) with *DAT-CreER* mice to generate *DAT-CreER* and wild-type littermates; we also crossed *C57Bl6j* mice with *TPH2-CreER* mice to generate *TPH2-CreER* and wild-type littermates.

Furthermore, we crossed $Drd1^{fl/fl}$ mice (Jackson Laboratory, 025700)[56] and *TPH2-CreER* mice to generate $Drd1^{fl/fl}$/*TPH2-CreER* mice ($DRD1^{TPH2}$-KO) and their littermate controls ($Drd1^{fl/fl}$). Similarly, we crossed $Drd2^{fl/fl}$ mice (Jackson Laboratory, 020631)[45] and *TPH2-CreER* mice to generate $Drd2^{fl/fl}$/*TPH2-CreER* mice and their littermate controls ($Drd2^{fl/fl}$). All mice received tamoxifen inductions (0.2 mg g^{-1}, intraperitoneal) at 8 weeks of age. Some $Drd1^{fl/fl}$ mice or $Drd2^{fl/fl}$ mice were anesthetized by isoflurane and received stereotaxic injections of AAV8-hSyn-GFP-Cre (6.5×10^{12} genome copies per milliliter (GC ml^{-1}), UNC Gene Therapy Center) into the DRN (400 nl), and these mice were referred as $DRD1^{DRN}$-KO or $DRD2^{DRN}$-KO. $Drd1^{fl/fl}$ mice or $Drd2^{fl/fl}$ mice that received AAV8-hSyn-GFP (5.6×10^{12} GC ml^{-1}, UNC Gene Therapy Center) in the DRN were used as controls. At the end of the experiment, all mice were perfused with 10% formalin. Brain sections were collected, and expression of GFP was checked in the DRN. Only those with expression of GFP exclusively in the DRN were included in data analyses.

$TPH2^{fl/fl}$ mice (Jackson Laboratory, 027590)[57] were injected with sustained-release buprenorphine 1 mg kg^{-1} and meloxicam 4 mg kg^{-1} before the surgery and meloxicam 4 mg kg^{-1} each day for 3 days after the surgery as analgesics. The mice were anesthetized by isoflurane and received stereotaxic injections of AAV8-hSyn-GFP-Cre (6.5×10^{12} GC ml^{-1}, UNC Gene Therapy Center) into the DRN (400 nl), and these mice were referred as $TPH2^{DRN}$-KO. $TPH2^{fl/fl}$ mice that received AAV8-hSyn-GFP (5.6×10^{12} GC ml^{-1}, UNC Gene Therapy Center) in the DRN were used as controls. Note that, because we observed that 5-HT^{DRN} neurons co-expressing DRD1 and DRD2 mRNAs are concentrated on the medial DRN (mDRN), we injected the virus into the midline of the DRN to delete TPH2 in this region. At the end of the experiment, all mice were perfused with 10% formalin. Brain sections were collected, and expression of GFP and TPH2 immunoreactivity were checked in the DRN.

All the breeders have been back-crossed to C57Bl6j background for more than 12 generations. Mice were housed in a temperature-controlled environment in groups of 2–5 at 22−24 °C using a 12-hour light/dark cycle. All mice were fed standard chow (6.5% fat, 2920, Harlan Teklad) ad libitum, unless described otherwise. Water was provided ad libitum.

RNAscope.

Mice were anesthetized and perfused with 0.9% saline followed by 10% formalin. Brains were removed and post-fixed in 10% formalin for 16 hours at 4 °C and cryoprotected in 30% sucrose for 48 hours. Brains were frozen and sectioned at 14 μm using the cryostat and washed in DEPC-treated PBS for 10 minutes. Sections were mounted on charged slides,

dried for 0.5 hours at room temperature and stored at −80 °C. On the day of the RNAscope assay, the slides were thawed and rinsed two times in PBS and baked in an oven for 30 minutes at 60 °C. After that, slides were post-fixed in 10% formalin for 15 minutes at 4 °C. Slides were then gradually dehydrated in ethanol (50%, 70% and 100%, 5 minutes each) and underwent target retrieval for 5 minutes at 100 °C. After being incubated in protease III (322337, Advanced Cell Diagnostics) for 30 minutes at 40 °C, slides were rinsed in distilled water and incubated in mouse RNAscope probes for *Tph2* (318691, Advanced Cell Diagnostics; Supplementary Table 1), *Drd1* (416901-C3, Advanced Cell Diagnostics; Supplementary Table 1) and *Drd2* (406501-C2, Advanced Cell Diagnostics; Supplementary Table 1) for 2 hours at 40 °C. Sections were then processed using RNAscope Fluorescent Multiplex Detection Reagents (320851, Advanced Cell Diagnostics) according to the manufacturer instructions. Slides were cover-slipped and analyzed using a Leica DM5500 fluorescence microscope with OptiGrid structured illumination configuration.

Optogenetics and fasting-induced refeeding.

We stereotaxically injected AAV-EF1α-DIO-hChR2(H134R)-EYFP into the VTA (200 nl, 6.2×10^{12} GC ml^{-1}; Supplementary Table 1) of *DAT-CreER* (with tamoxifen induction, 0.2 mg g^{-1}, intraperitoneal) to express ChR2 specifically in DA^{VTA} neurons and their fibers and terminals. During the same surgery, an optic fiber (200-μm core, 0.39 NA, CFML12U-20, Thorlabs) was implanted to aim the DRN (4.65 mm posterior, 0 mm lateral and 3.3 mm ventral to bregma), which allows photostimulation of the DA^{VTA}→DRN circuit. After a 4-week recovery, mice were singly housed in their home cages[58]. After acclimation, mice were fasted overnight. The next morning, regular chow (6.5% fat, 2020, Harlan Teklad) was provided back to the cages. During the first hour of refeeding, blue light (473 nm, 10 ms per pulse; MGL-FN-589, CNI LASER) was used to stimulate the circuit. Various frequencies (2 Hz, 5 Hz or 20 Hz) of photostimulation protocols were applied to these mice in different trials, and yellow light (595 nm, 10 ms per pulse; MGL-FN-589, CNI LASER) at 2 Hz, 5 Hz or 20 Hz was used as controls, respectively. Food intake was monitored. In a different cohort of mice, we implanted a guide cannula (C200GS-5/SPC with a terminal length of 3.5 mm, P1 Technologies) to aim the DRN using the same coordinates. An optic fiber (200-μm core, 0.39 NA; FT200EMT, Thorlabs) was assembled with a Stainless Steel Ferrule (SFLC230–10, Thorlabs), a Housing (C200H, P1 Technologies) and a Fiber-Cap (303/OFC, P1 Technologies) using Resin Adhesive (2 Part Epoxy, Gorilla Glue Company). An internal cannula (C200IS-5/SPC customized to fit 3.5-mm C200GS-5/SPC with 0.5-mm projection, P1 Technologies) was used for drug infusion, and the assembled optic fiber cap (fiber cut to fit 3.5-mm C200GS-5/SPC with no projection) was used for photostimulation, as described by others[59]. After an overnight fasting, mice received an intra-DRN injection of saline (200 nl), SCH23390 (10 ng in 200 nl of saline, the DRD1 inhibitor; Supplementary Table 1)[60] or eticlopride (100 ng in 200 nl saline, the DRD2 inhibitor; Supplementary Table 1)[61]. One hour later, food was provided, and the 1-hour photostimulation (blue or yellow light at 2 Hz or 20 Hz) was applied as described above. Food intake was monitored. To evaluate the involvement of $5\text{-}HT^{DRN}$ neurons in mediating 20-Hz blue-light-induced changes in food intake, we injected AAV-EF1α-DIO-hChR2(H134R)-EYFP into the VTA and AAV-hSyn-DIO-hM4D(Gi)-mCherry into the DRN in *DAT-CreER/ TPH2-CreER* mice to express ChR2 in DA^{VTA} neurons and hM4Di in $5\text{-}HT^{DRN}$ neurons. During the same

surgery, an optic cannula was implanted to target the DRN, which allowed photostimulation of the $DA^{VTA}\rightarrow$DRN circuit. After recovery and acclimation, mice were fasted overnight and received saline or CNO injection half an hour before they were subjected to a 1-hour yellow or blue light stimulation at 20 Hz. Once the stimulation started, regular chow was provided, and food intake was measured. In these aforementioned experiments, the same mice received multiple treatments (photostimulations plus drug injections) in different trials, and each trial was for one different treatment. There was no repeat of the same treatment on the same mouse. Notably, all these trials were performed on different days separated by 6-day intervals to ensure 'wash out' of previous treatment. In addition, we always conducted these experiments in the morning to avoid confounding effects from the circadian cues.

To confirm the effects of the $DA^{VTA}\rightarrow$DRN projections, we injected the AAV-EF1α-DIO-hChR2(H134R)-EYFP virus into a different cohort of wild-type and *DAT-CreER* mice. After recovery and acclimation, mice were fasted overnight and subjected to a 5-minute block of blue light-on followed by a 5-minute block of blue light-off at 2 Hz or 20 Hz for three consecutive times. During these light-on and light-off blocks, regular chow was continuously provided, and food intake was monitored for each block.

Real-time conditioned place preference test.

The same mice used in the aforementioned optogenetic studies were used here. All tests were performed in a dedicated soundproof behavioral facility. These mice were brought to the procedure room 1 hour before the start of each test and remained in the same room throughout the test. At all times, sound was masked with 60–65 Db of white noise. The conditioned place preference apparatus contained two identical conditioning chambers (chambers 1 and 2) that were connected by an opening (12.5 cm) in the center. Each chamber was 50 × 50 × 25 cm (length × width × height) with a black pexiglass wall and a white pexiglass floor. The same mice received multiple photostimulations in different trials. In each trial, mice were allowed to explore the two chambers for half an hour during the light cycle. We first performed up to five training sessions to ensure that mice showed relatively equal preference to each of the chambers when there was no coupling to the optogenetic stimulation or to food. Then, blue light (473 nm, 10 ms per pulse; 2 Hz, 5 Hz or 20 Hz) was shed whenever the mouse entered chamber 2 and ceased when it entered chamber 1. In some trials, chow pellets were placed in chamber 1. Time spent in each chamber was recorded and analyzed for chamber preference by experimenters blinded to experimental information. At end of these experiments, all mice were perfused with 10% formalin. Brain sections were collected, and expression of EYFP was checked in the VTA. The track of optic fibers was examined in the DRN. Only those with accurate targeting were included for data analyses. Note that both male and female mice were included in these feeding studies and the real-time conditioned place preference test. Because we did not observe any sex differences in the endpoints, we pooled male and female data together for analyses.

ABA.

Because AN is more prevalent in women than in men, and female rodents are more prone to develop AN-like behavior in the ABA paradigm, we used female mice for all ABA studies.

All the ABA studies were performed in cohorts of littermates, such that data presented in each figure were generated from mice of the same age and the same sex (all females). Before beginning the ABA protocol[33,62], various mutant mice and their littermate controls were singly housed and acclimated to the home cages equipped with running wheels (Columbus Instruments) for 3 days. After acclimation, mice were maintained in the same cages with running wheels for five additional days with unrestricted access to the regular chow and water. Food intake and body weight were measured daily just before the beginning of the dark cycle (18:00). Then, mice were subjected to a restricted feeding schedule (the ABA period) for 5 days (1 hour of daily access to food from 18:00 to 19:00), with free access to water and running wheels. Food and body weight were measured daily at 18:00 and 19:00. Individual wheel running revolutions were continuously registered using Cage Registration software (Columbus Instruments). Mice losing more than 20% of their original body weight were immediately euthanized per the Institutional Animal Care and Use Committee protocol and counted as 'mortality'. Because many mice were removed from the study on different days of the ABA period, it was difficult to compare food intake and running wheel activity on the same day during the ABA period. To cope with this issue, we first calculated the averaged daily food intake and running wheel activity during days 2–5 for each mouse and used this value to reflect the mouse's food intake and running wheel activity during the ABA period. To examine the effects of gene deletion (for example, *Drd1* or *Drd2* deletion), the deletion mice and their control littermates were subjected to the ABA paradigm as described above. To examine the effects of SCH23390 on ABA phenotypes, wild-type mice were subjected to the ABA paradigm described above, with a modification that they received intraperitoneal injections of SCH23390 (0.1 mg kg^{-1}) at 17:30 every day.

DREADD.

Female *DAT-CreER* mice and wild-type littermates mice (at 8–10 weeks of age) were anesthetized by isoflurane and received stereotaxic injections of retrograde AAVretro-hM4Dq-mCherry (pAAV-hSyn-DIO-hM4D(Gi)-mCherry (AAV Retrograde), 1.3×10^{13} viral genomes per milliliter (VG ml^{-1}); Addgene, 44362-AAVrg; Supplementary Table 1) into the DRN (400 nl). Similarly, female *TPH2-CreER* mice and wild-type littermates mice (at 8–10 weeks of age) were anesthetized by isoflurane and received stereotaxic injections of AAV-hM4Dq-mCherry (AAV-hSyn-DIO-hM4D(Gi)-mCherry in AAV2, 5.9×10^{12} VG ml^{-1}, UNC Vector Core; Supplementary Table 1) into the DRN (400 nl). After tamoxifen induction (0.2 mg g^{-1}, intraperitoneal) and a 4-week recovery, mice were subjected to the ABA paradigm described above, with a modification that they received intraperitoneal injection of CNO (3 mg kg^{-1}, 16882, Cayman Chemical; Supplementary Table 1) at 17:30 every day. At the end of experiment, all mice were perfused with 10% formalin. Brain sections were collected and directly mounted on glass slides. mCherry fluorescence was analyzed using a Leica DM5500 fluorescence microscope with OptiGrid structured illumination configuration. Only those with mCherry signals in the VTA or DRN were included in data analyses. To prove the concept that CNO does inhibit hM4Di-mCherry-expressing DA^{VTA} neurons or $5\text{-}HT^{DRN}$ neurons, some mice were used for slice electrophysiology (as described below) to measure responses in firing frequency and resting membrane potential in response to 10 μM CNO treatment.

Slice electrophysiology.

To examine the activities of DRN-projecting DA^{VTA} neurons, 12-week-old *DAT-CreER/Rosa26-LSL-tdTOMATO* mice received stereotaxic injections of Green RetroBeads (200 nl; Supplementary Table 1) into the DRN. In this case, tdTOMATO-labeled VTA neurons that contained the Green RetroBeads were identified as DRN-projecting DA^{VTA} neurons. *TPH2-CreER/Rosa26-LSL-tdTOMATO* mice (after tamoxifen induction, 0.2 mg g^{-1}, intraperitoneal) were used to record tdTOMATO-labeled 5-HT^{DRN} neurons. Because we observed that 5-HT^{DRN} neurons co-expressing DRD1 and DRD2 mRNAs are more concentrated on the mDRN, we focused our recordings on 5-HT^{DRN} neurons in this region. We compared the neural activity of DRN-projecting DA^{VTA} neurons or 5-HT^{DRN} neurons in naive or ABA mice. For ABA mice, they were exposed to the ABA paradigm as described above. On day 2, they were euthanized at 18:00 immediately before the restricted feeding would start. As controls, naive mice were fed ad libitum without any exposure to running wheels; then, they were fasted from 18:00 and euthanized at 18:00 on the next day, followed by slice recordings.

Mice were deeply anesthetized with isoflurane and transcardially perfused with a modified ice-cold sucrose-based cutting solution (pH 7.3) containing 10 mM NaCl, 25 mM $NaHCO_3$, 195 mM sucrose, 5 mM glucose, 2.5 mM KCl, 1.25 mM NaH_2PO_4, 2 mM Na-pyruvate, 0.5 mM $CaCl_2$ and 7 mM $MgCl_2$, bubbled continuously with 95% O_2 and 5% CO_2. The mice were then decapitated, and the entire brain was removed and immediately submerged in the cutting solution. Slices (250 μm) were cut with a Microtome HM 650V vibratome (Thermo Fisher Scientific). Coronal brain slices containing the DRN or VTA were obtained for each animal. The slices were recovered for 1 hour at 34 °C and then maintained at room temperature in artificial cerebrospinal fluid (aCSF, pH 7.3) containing 126 mM NaCl, 2.5 mM KCl, 2.4 mM $CaCl_2$, 1.2 mM NaH_2PO_4, 1.2 mM $MgCl_2$, 5.0 mM glucose and 21.4 mM $NaHCO_3$ saturated with 95% O_2 and 5% CO_2 before recording. Slices were transferred to a recording chamber and allowed to equilibrate for at least 10 minutes before recording. The slices were superfused at 34 °C in oxygenated aCSF at a flow rate of 1.8–2 ml min^{-1}. tdTOMATO and/or beads-labeled neurons were visualized using epifluorescence and IR-DIC imaging on an upright microscope (Eclipse FN-1, Nikon) equipped with a movable stage (MP-285, Sutter Instrument). Patch pipettes with resistances of 3–5 MΩ were filled with intracellular solution (pH 7.3) containing 128 mM K-gluconate, 10 mM KCl, 10 mM HEPES, 0.1 mM EGTA, 2 mM $MgCl_2$, 0.05 mM Na-GTP and 0.05 mM Mg-ATP. Recordings were made using a MultiClamp 700B amplifier (Axon Instruments), sampled using Digidata 1440A and analyzed offline with pClamp 10.3 software (Axon Instruments). Series resistance was monitored during the recording, and the values were generally <10 MΩ and were not compensated. The liquid junction potential was +12.5 mV and was corrected after the experiment. Data were excluded if the series resistance increased markedly during the experiment or without overshoot for action potential. Currents were amplified, filtered at 1 kHz and digitized at 20 kHz. Current clamp was engaged to test neural firing frequency and resting membrane potential[63]. The values were averaged within a 2-minute bin. Because DA neurons periodically exhibited phasic bursting, the firing frequency and resting membrane potential were analyzed in a 2-minute bin when no bursting event was present to better reflect the tonic firing properties. In addition, bursting activity

was also specifically analyzed by calculating bursting score (bursting event frequency × number of spikes per burst)[64]. Bursts were identified as discrete events consisting of a sequence of spikes such that their onset was defined by two consecutive spikes within an interval lower than 80 ms whenever they terminated with an interval greater than 160 ms[64].

To examine effects of dopamine on 5-HT^{DRN} neurons, we puff treated (500 ms) the 5-HT^{DRN} neurons with different concentrations of DA, including 0.001, 0.01, 0.05, 0.1, 0.2, 0.4, 0.6, 0.8, 1.0 and 10 μM in the presence of cocktail blockers (30 μM D-AP5, 30 μM CNQX and 50 μM bicuculline in the bath perfusion solution; Supplementary Table 1), respectively. Because we found that 0.05 μM clearly hyperpolarized 5-HT^{DRN} neurons, whereas 10 μM dopamine depolarized 5-HT^{DRN} neurons, we then recorded the effects of 0.05 μM dopamine (puff) or 10 μM dopamine (bath perfusion) in the presence of bath perfusion of cocktail blockers (30 μM D-AP5, 30 μM CNQX and 50 μM bicuculline), with or without a 30-minute pre-incubation of 5 μM SCH23390 (a DRD1 antagonist) or 20 μM eticlopride (a DRD2 antagonist)[65]. Whole-cell patch-clamp recording was also used to validate the functional deletion of *Drd1* and *Drd2* in 5-HT neurons. To validate DRD1^{DRN}-KO, we treated 5-HT^{DRN} neurons from control or DRD1^{DRN}-KO mice with the DRD1 selective agonist SKF38393 (1 μM, 500 ms puff; Supplementary Table 1). The DRD2 selective agonist quinpirole (5 μM, 500 ms puff; Supplementary Table 1) was used to treat 5-HT^{DRN} neurons from control or DRD2^{DRN}-KO mice to validate DRD2^{DRN}-KO.

We modified the channelrhodopsin-2 (ChR2)-assisted circuit mapping approach[66,67] to examine the neurotransmissions between DA^{VTA} neurons and 5-HT^{DRN} neurons. In brief, 12-week-old *TPH2-CreER/DAT-CreER/Rosa26-LSL-tdTOMATO* mice were anesthetized by isoflurane and received stereotaxic injections of Ad-iN/WED (obtained from Martin Myers at the University of Michigan, 100 nl per site; Supplementary Table 1) and AAV-EF1α-DIO-hChR2(H134R)-EYFP (6.2×10^{12} GC ml^{-1}, 100 nl per site) into the VTA. Tamoxifen (0.2 mg g^{-1}, intraperitoneal) was injected into these mice to induce Cre recombinase activity. After a 4-week recovery, mice were sacrificed, and unfixed brain slices (containing both the DRN and VTA, 250 μm in thickness) were prepared from these mice. Ad-iN/WED expressed GFP-tagged wheat germ agglutinin (WGA-GFP) in a Cre-dependent manner, and, therefore, only DA^{VTA} neurons were filled with WGA-GFP. WGA-GFP is an anterograde trans-synaptic tracer[30], which labels the downstream neurons that are innervated by DA^{VTA} neurons. Thus, GFP-labeled neurons in the DRN were identified as putative targets of DA^{VTA} neurons. Furthermore, the *TPH2-CreER* and *Rosa26-LSL-tdTOMATO* alleles labeled 5-HT neurons with red tdTOMATO fluorescence. These brain slices were used to perform electrophysiological recordings from WGA^{+}/tdTOMATO^{+} neurons in the DRN. Under the current-clamp mode, 30 μM D-AP5, 30 μM CNQX and 50 μM bicuculline were applied in the bath solution to block the glutamate and GABA inputs. Action potential firing frequency and resting membrane potential were recorded in response to blue light (473 nm, 10 ms pulse, 0.2 mW) at different frequencies (2 Hz, 5 Hz, 10 Hz, 20Hz and 30 Hz). Some recordings were made in the presence of 100 μM SCH23390 or 100 μM eticlopride by bath perfusion[65].

Fiber photometry.

To record activity of DRN-projecting DA^{VTA} neurons in freely moving mice, female *DAT-CreER* mice (12 weeks of age) were anesthetized by isoflurane and received stereotaxic injections of retrograde HSV-hEF1α-LS1L-GCaMP6f (HSV-hEF1α-LS1L-GCaMP6f-RN506, 3×10^9 VG ml^{-1}; MGH Gene Delivery Technology Core; Supplementary Table 1) into the DRN (400 nl). During the same surgery, an optical fiber (fiber: core = 400 μm, 0.48 NA, M3 thread titanium receptacle; Doric Lenses) was implanted over the VTA (3 mm posterior, 0.5 mm lateral and 4.3 mm ventral to bregma). Similarly, female *TPH2-CreER* or $DRD1^{TPH2}$-KO mice (12 weeks of age) were anesthetized by isoflurane and received stereotaxic injections of pAAV9.Syn.Flex.GCaMP6m WPRE.SV40 (400 nl per site, 3×10^9 viral particles per milliliter (VP ml^{-1}); Supplementary Table 1) into the DRN. During the same surgery, an optical fiber (fiber: core = 400 μm, 0.48 NA, M3 thread titanium receptacle; Doric Lenses) was implanted over the DRN (4.65 mm posterior, 0 mm lateral and 3.30 mm ventral to bregma). Fibers were fixed to the skull using dental acrylic. Mice received tamoxifen inductions (0.2 mg g^{-1}, intraperitoneal) 1 week later and were individually housed for at least 4 weeks before acclimating to investigator's handling for 1 week before the recordings. To measure DA levels in the DRN in freely moving mice, female C57Bl6j mice (12 weeks of age) were anesthetized by isoflurane and received stereotaxic injections of pAAV-hSyn-GRAB_DA1h (113050-AAV9, 2.4×10^{13} GC ml^{-1}, Addgene; Supplementary Table 1) into the DRN (200 nl). During the same surgery, an optical fiber (fiber: core = 400 μm, 0.48 NA, M3 thread titanium receptacle; Doric Lenses) was implanted over the DRN. Mice were individually housed for at least 4 weeks before acclimating to investigator's handling for 1 week before the recordings.

Mice were allowed to adapt to the tethered patchcord for 2 days before experiments and given 5 minutes to acclimate to the tethered patchcord before any recording. Recordings were done in mice at two different conditions: naive or ABA. In each condition, there were several different nutritional states—for example, Ad Libitum (only at naive condition), Fasted, Refed 30 minutes or Refed 60 minutes. The naive condition was done before mice went through the ABA protocol. At this condition, mice were fed ad libitum without any exposure to running wheels, and a 5-minute recording was performed during 17:55–18:00; this was denoted as the 'Ad Lib' state. Then, the mice were fasted for 24 hours (18:00–18:00); at the end of this fast, a 5-minute recording was performed during 17:55–18:00, denoted as the 'Fasted' state. Food was then provided back to the cage at 18:00. While mice were refeeding, several 5-minute recordings were performed every 30 minutes, and these were denoted as 'Refed 30 minutes' or 'Refed 60 minutes'. These mice were then subjected to the ABA paradigm as described above. On day 2 of the ABA period, several 5-minute recordings were performed every 30 minutes during the feeding period. Note that, because ABA mice were never fed ad libitum, there were no data at the 'Ad Lib' state for mice at the ABA condition. Because the fiber photometry recording was not compatible with the running wheel, the running wheel was temporarily removed from the cage during the 5-minute recordings.

For each recording, continuous <20 μW blue LED at 465 nm and UV LED at 405 nm served as excitation light sources, driven by a multichannel hub (Doric Lenses), modulated

at 211 Hz and 330 Hz, respectively. The light was delivered to a filtered minicube (FMC5, Doric Lenses) before connecting through optic fibers to a rotary joint (FRJ 1 × 1, Doric Lenses) to allow for movement. GCaMP6 calcium GFP signals (or GRAB_DA1h) and UV autofluorescent signals were collected through the same fibers back to the dichroic ports of the minicube into a femtowatt silicon photoreceiver (2151, Newport). The digital signals were then amplified, demodulated and collected through a lock-in amplifier (RZ5P, Tucker-Davis Technologies)[68]. The fiber photometry data were downsampled to 8 Hz. To align acute neural responses (in seconds) to each eating bout, animals' behavior was also simultaneously recorded with an infrared camera. We derived the values of GCaMP6 (or GRAB_DA1h) fluorescence change ($\Delta F/F_0$) by calculating ($F_{465} - F_0$) / F_0, where F_0 is the baseline fluorescence of the F_{465} channel signal 2–5 seconds before the onset of each eating bout[69]. The F_{405} channel is used as an isosbestic fluorescence channel. We derived the values of isosbestic fluorescence change ($\Delta F/ F_0$) by calculating ($F_{405} - F_0$) / F_0, where F_0 is the baseline fluorescence of the F_{405} channel signal 2–5 seconds before the onset of each eating bout. To evaluate the slow changes in neural activity (5-minute bin for every 30 minutes), we derived the values of fluorescence change ($\Delta F/F_n$) by calculating ($F_{465} - F_{405}$) / F_{405} to minimize the interference of movement and/or bleaching artifacts[34].

Immunohistochemistry.

The brain sections were cut at 25 μm and collected into five consecutive series. One series of the sections were blocked (3% normal donkey or goat serum) for 1 hour and incubated with mouse anti-tyrosine hydroxylase (TH) antibody (1:5,000, 22941, ImmunoStar; Supplementary Table 1) on a shaker at 4° for overnight, followed by the donkey anti-mouse Alexa Fluor 594 (1:200, A21203, Invitrogen; Supplementary Table 1) or goat anti-mouse Alexa Fluor 488 (1:200, A11001, Invitrogen; Supplementary Table 1) for 2 hours. Slides were cover-slipped and analyzed using a fluorescence microscope.

To check TPH2 distribution in *DAT-CreER/Rosa26-LSL-tdTOMATO* mice, the brain sections were blocked (3% normal donkey serum) for 1 hour and incubated with rabbit anti-TPH2 antibody (1:3,000, Ab111828, Abcam[70]; Supplementary Table 1) on a shaker at room temperature for overnight, followed by the donkey anti-rabbit Alexa Fluor 488 (1:200, A21206, Invitrogen; Supplementary Table 1) for 2 hours. Slides were cover-slipped and analyzed using a fluorescence microscope.

To evaluate the close apposition of EYFP fibers with 5-HT neurons, the brain sections from *DAT-CreER* mice that received AAV-EF1α-DIO-hChR2(H134R)-EYFP injection into the VTA were blocked (3% normal donkey serum) for 1 hour and incubated with rabbit anti-5-HT antibody (1:5,000, 20080, ImmunoStar; Supplementary Table 1) on a shaker at room temperature for overnight, followed by the donkey anti-rabbit Alexa Fluor 594 (1:200, A21207, Invitrogen; Supplementary Table 1) for 2 hours. Slides were cover-slipped and analyzed using a fluorescence microscope.

To examine TPH2 immunoreactivity, the brain sections were blocked (3% normal goat serum) for 1 hour and incubated with rabbit anti-TPH2 antibody (1:3,000, Ab111828, Abcam[70]) on a shaker at room temperature for overnight, followed by the goat anti-rabbit

Alexa Fluor 405 (1:200, A31556, Invitrogen[71]; Supplementary Table 1) for 2 hours. Slides were cover-slipped and analyzed using a fluorescence microscope.

Statistics.

The minimal sample size was pre-determined by the nature of experiments. No statistical methods were used to pre-determine sample sizes, but our sample sizes are similar to those reported in previous publications[16,18]. For most of physiological readouts (body weight, food intake, running wheel activity, etc.), 5–12 different mice per group were included. For histology studies, the same experiment was repeated in at least three different mice. For electrophysiological studies, at least 13 different neurons from three different mice were included. Allocation of organisms and brain slices into experimental groups was done at random. All conditions were randomly counterbalanced across organisms and brain slices. In experiments where grouping was determined by animals' genotyping, randomization was not practiced. The experimenter was blinded to genotype/experimental group before and during all experiments. No data were excluded. The data are presented as mean ± s.e.m. and/or as individual data points. Statistical analyses were performed using GraphPad Prism software to evaluate normal distribution and variations within and among groups. Methods of statistical analyses were chosen based on the design of each experiment and are indicated in the figure legends. $P < 0.05$ was considered to be statistically significant.

Study approval.

Care of all animals and procedures were approved by the Baylor College of Medicine Institutional Animal Care and Use Committee.

Reporting Summary.

Further information on research design is available in the Nature Research Reporting Summary linked to this article.

Extended Data

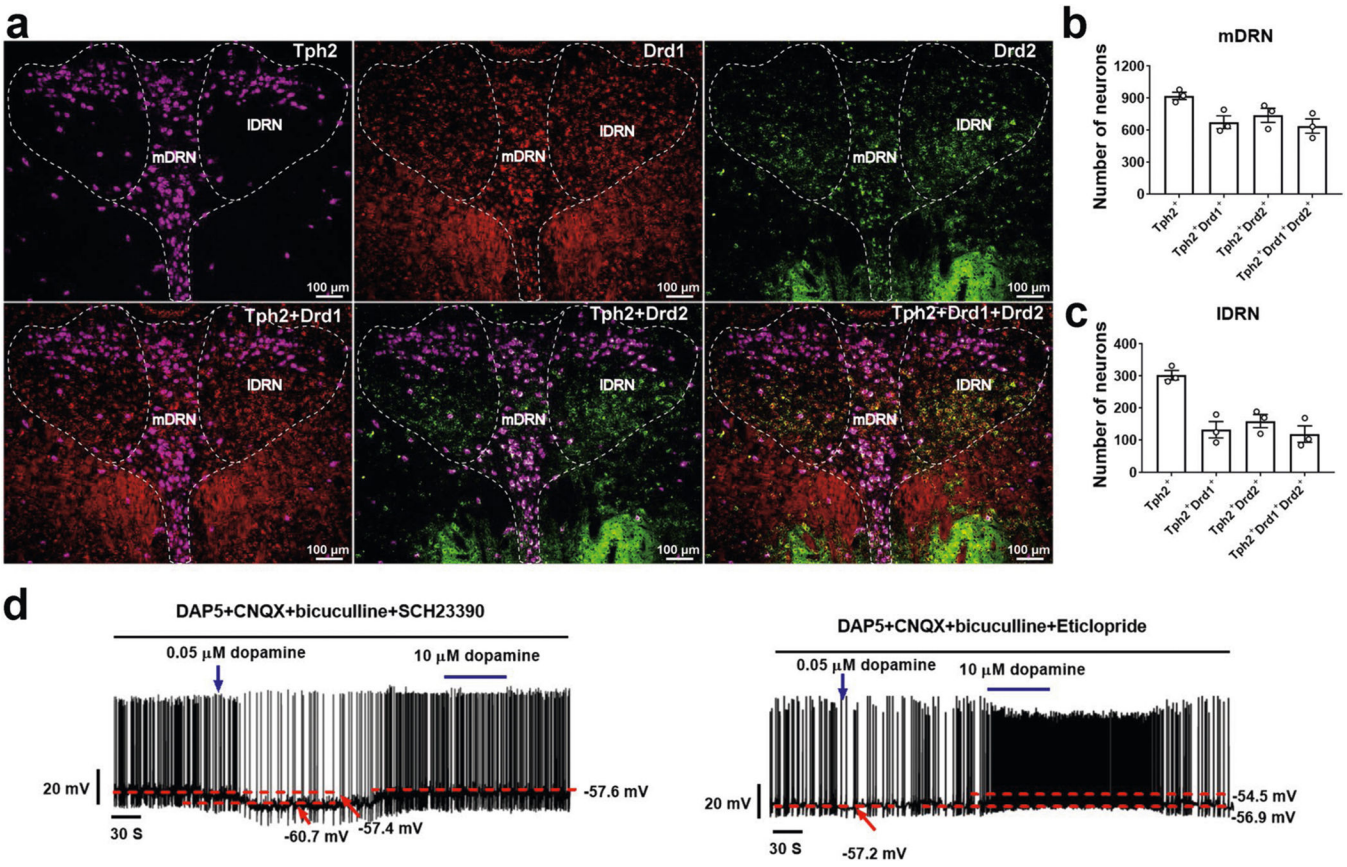

Extended Data Fig. 1 |. Distribution of Drd1 and Drd2 in 5-HT^{DRN} neurons.

(a) Representative RNAscope microscopic images showing *Tph2*, *Drd1*, *Drd2* mRNAs, and their co-localizations, in the mDRN and lDRN. Scale bars = 100 μm. (b-c) Quantification of the number of Tph2+ neurons co-expressing *Drd1* alone, *Drd2* alone or both in the mDRN **(b)** and lDRN **(c)**. Results are shown as mean ± s.e.m. with individual data points (n = 3 mice per group). lDRN, lateral DRN; mDRN, medial DRN. **(d)** Typical action potential traces of 5-HT^{DRN} neurons in response to DA (0.05 μM puff or 10 μM bath perfusion) in the presence of various inhibitors as indicated.

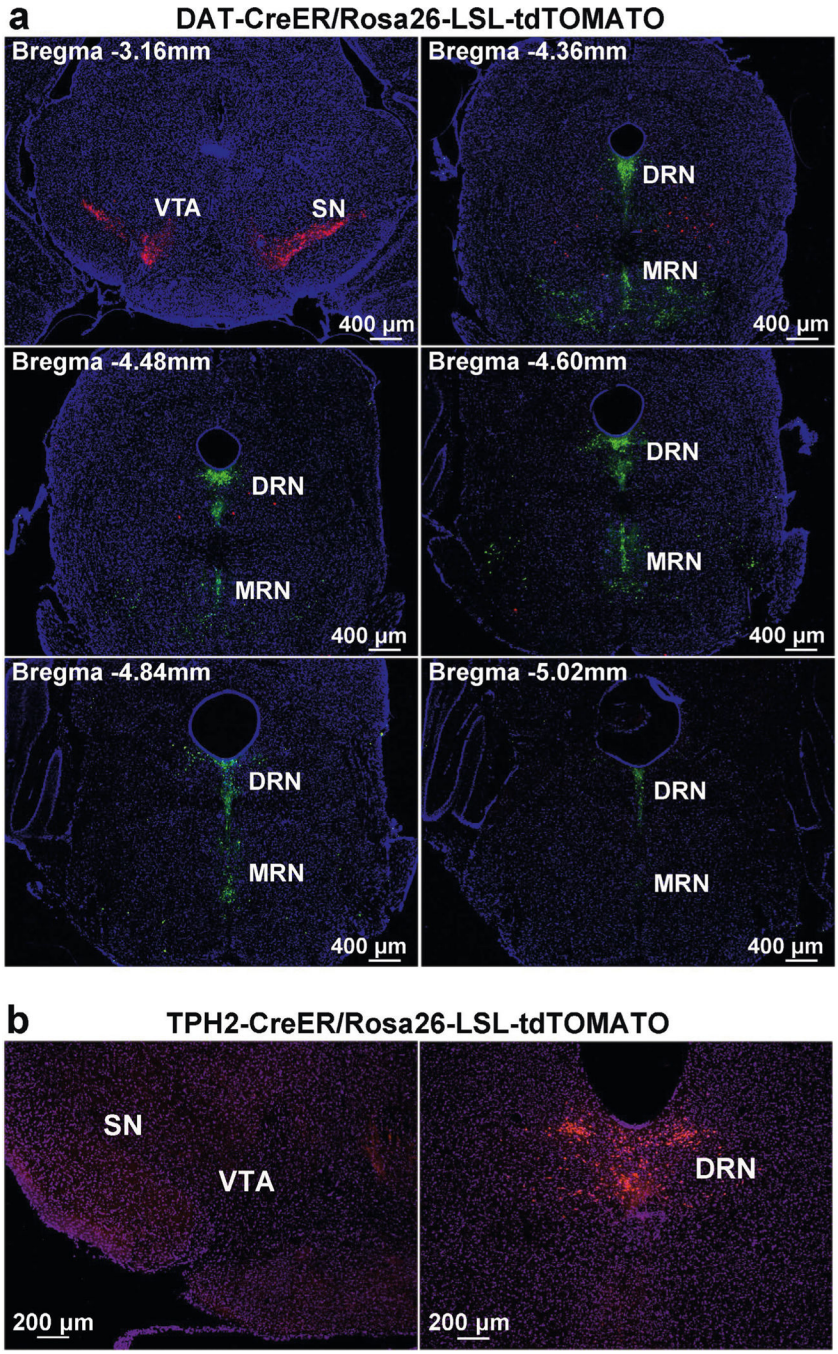

Extended Data Fig. 2 |. Distribution of tamoxifen-induced Cre activity in *DAT-CreER* mice and in *TPH2-CreER* mice.

(a) Representative microscopic images with DAPI counter staining showing the presence or absence of tdTOMATO signals (red) in the VTA, SN, DRN and MRN in *DAT-CreER/Rosa26-LSL-tdTOMATO* mice. These imaging studies were repeated in 3 mice. **(b)** Representative microscopic images with DAPI counter staining showing the presence or absence of tdTOMATO signals (red) in the VTA, SN and DRN in *TPH2-CreER/Rosa26-LSL-tdTOMATO* mice. These imaging studies were repeated in 3 mice. Scale bars are

indicated in each panel. DRN, dorsal Raphe nucleus; MRN, median Raphe nucleus; SN, substantia nigra; VTA, ventral tegmental area. Scale bars are indicated in each panel.

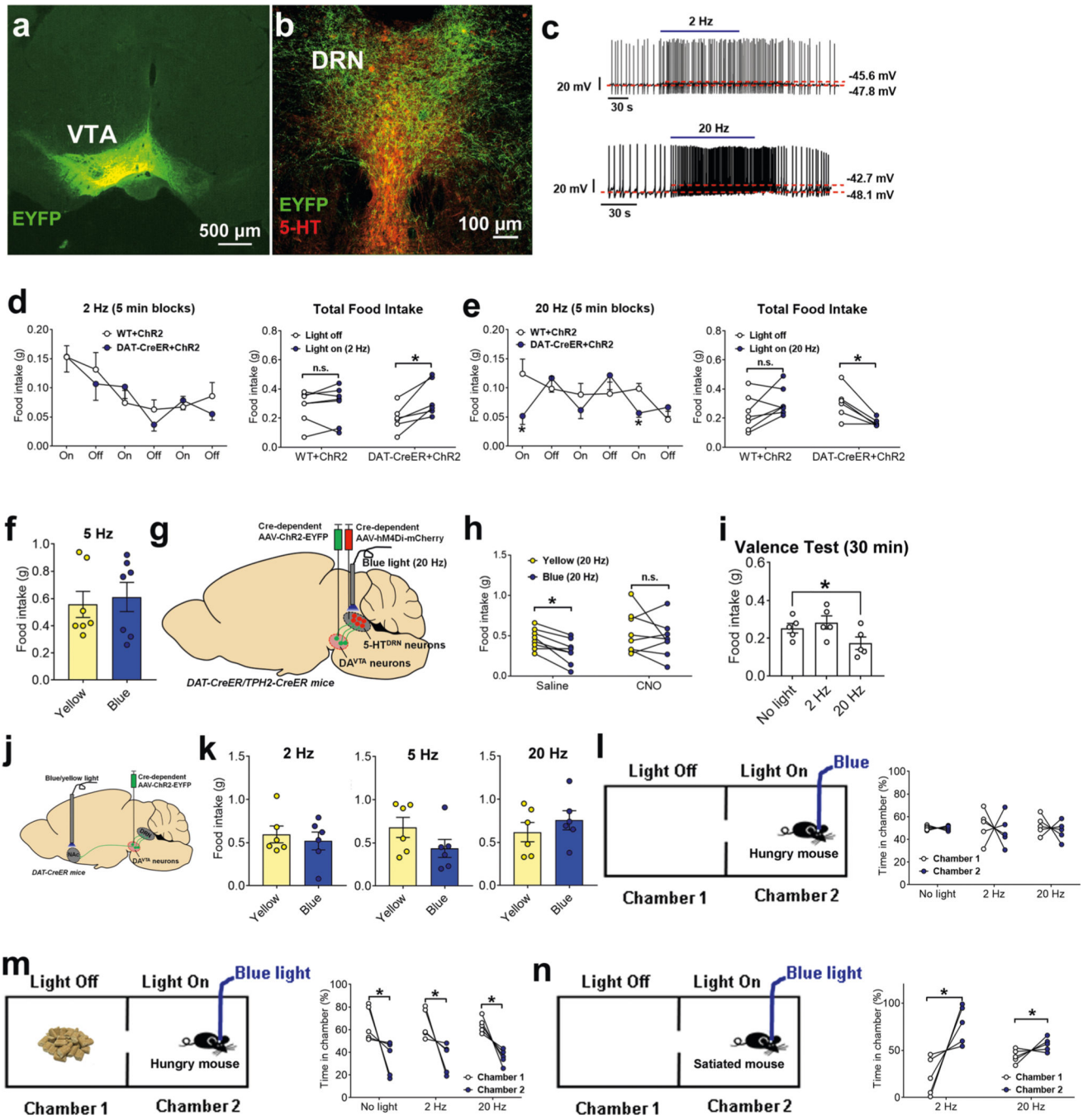

Extended Data Fig. 3 |. Bidirectional effects of the DA^{VTA}→DRN circuit on feeding.

(a-b) Representative images showing EYFP-labelled cell bodies and fibers within the VTA **(a)** and EYFP-labelled fibers in the DRN (b, repeated in 3 mice. **(c)** Typical action potential traces of ChR2-expressing DA^{VTA} neurons in response to 2 or 20 Hz photostimulation (repeated in 3 mice). **(d)** Left panel: refeeding in each of 5-min blocks when 2 Hz blue

light was turned on or off. Right panel: total refeeding during the 15-min periods. Results are shown as mean ± s.e.m., $*P < 0.05$ in two-sided unpaired t-tests (n = 6 or 7 mice per group). **(e)** Left panel: refeeding in each of 5-min blocks when 20 Hz blue light was turned on or off. Right panel: total refeeding during the 15-min periods. Results are shown as mean ± s.e.m., $*P < 0.05$ at each 5-min block in two-sided unpaired t-tests (n = 6 or 7 mice per group). **(f)** Effects of 5 Hz photostimulation of the $DA^{VTA}\rightarrow$DRN projections on refeeding. Results are shown as mean ± s.e.m. with individual data points. n = 7 mice. **(g)** Strategy to activate the $DA^{VTA}\rightarrow$DRN projections and simultaneously inhibit $5\text{-}HT^{DRN}$ neurons. **(h)** Effects of 20 Hz photostimulation on refeeding after i.p. injections of saline or CNO. Results are shown as individual data points. $*P < 0.05$ in two-sided paired t-tests (n = 8 mice). **(i)** Food intake measured during the 30-min valence tests. Results are shown as mean ± s.e.m. with individual data points. $*P < 0.05$ in two-sided paired t-tests (n = 8 mice). **(j)** Strategy to activate the $DA^{VTA}\rightarrow$NAc projections. **(k)** Effects of 2, 5 and 20 Hz photostimulation of the $DA^{VTA}\rightarrow$NAc projections on refeeding. Results are shown as mean ± s.e.m. with individual data points (n = 6 mice). (l-n) Time spent in each chamber with or without blue light stimulation coupled to Chamber 2. Results are shown as individual data points. $*P <$ 0.05 in two-sided unpaired t-tests (n = 5 mice per group).

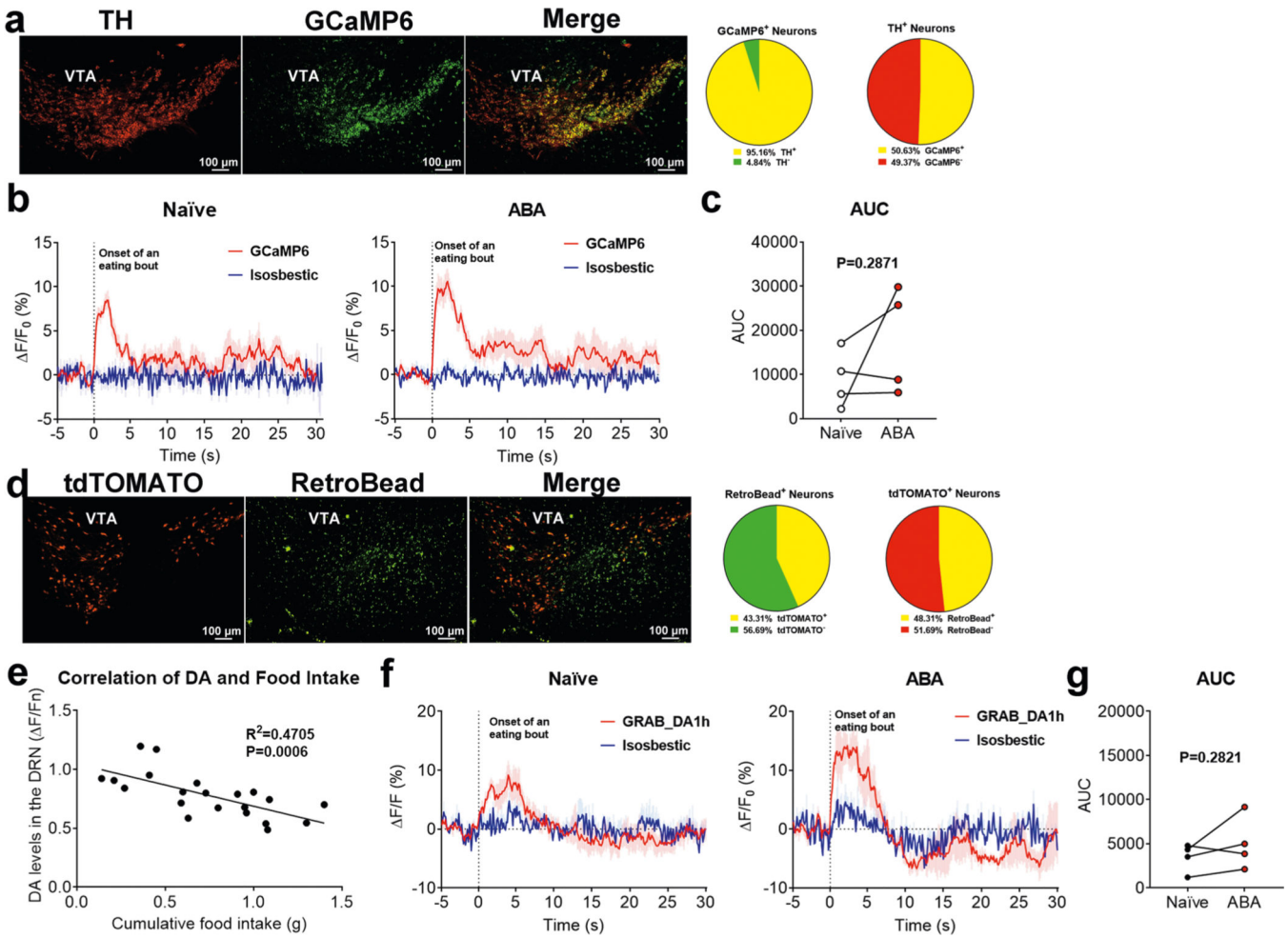

Extended Data Fig. 4 |. DRN-projecting DA^{VTA} neurons are activated during activity-based anorexia.

(a) Representative images showing TH-positive neurons within the VTA labelled by GCaMP6. Scale bars are indicated in each panel. Data from 3 different mice were quantified. VTA, ventral tegmental area. **(b)** Averaged GCaMP6 and isosbestic signals in DRN-projecting DA^{VTA} neurons associated with eating bouts in naïve and ABA mice. Results are shown as mean ± s.e.m. (n = 4 mice per group). **(c)** Area under the curves (10 seconds after eating bouts) of the GCaMP6 signals in **(b)**. Results are shown as individual data points (n = 4 mice per group). **(d)** Representative images showing tdTOMATO-positive neurons within the VTA labelled by Green RetroBeads. Scale bars are indicated in each panel. Data from 3 different mice were quantified. VTA, ventral tegmental area. **(e)** The linear regression curve of cumulative chow intake and DA levels in the DRN during refeeding. Results are shown as individual data points with the linear regression curve plotted. **(f)** Averaged GRAB_DA1h and isosbestic signals in the DRN associated with eating bouts in naïve and ABA mice. Results are shown as mean ± s.e.m. (n = 4 mice per group). **(g)** Area under the curves (10 seconds after eating bouts) of the GRAB_DA1h signals in **(F)**. Results are shown as individual data points (n = 4 mice per group).

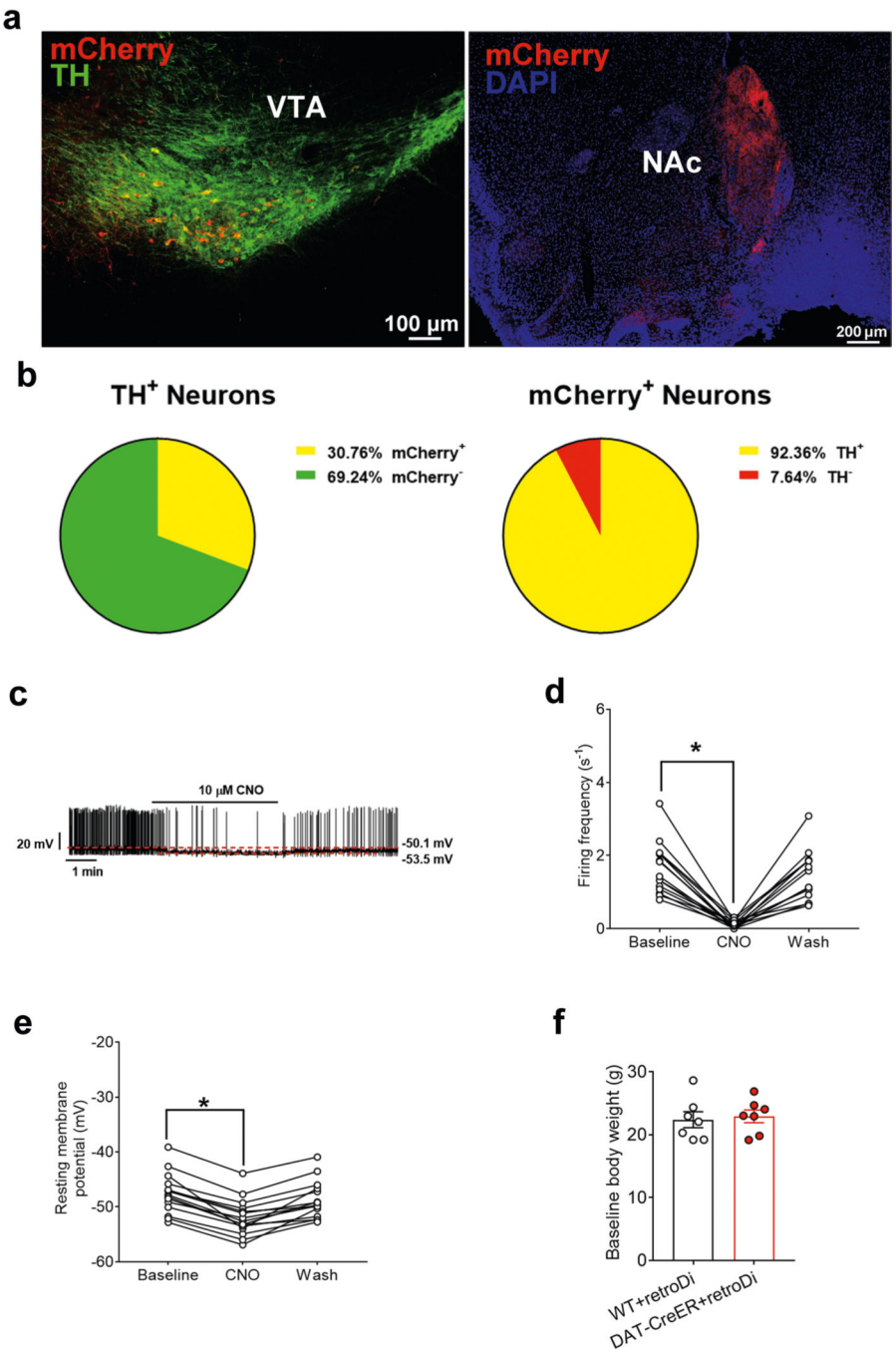

Extended Data Fig. 5 |. DRN-projecting DA^{VTA} neurons mediate activity-based anorexia. **(a)** Left: a representative image showing TH-positive neurons (green) within the VTA partially co-localize with mCherry (red). Right: a representative image showing mCherry-labelled collateral projections to the NAc. Scale bars are indicated in each panel. NAc, nucleus accumbens; VTA, ventral tegmental area. **(b)** Left: 30.76% of DA^{VTA} neurons (labelled by TH immunoreactivity) are positive for mCherry; right: 92.36% of mCherry-labelled neurons are positive for TH. Results were quantified from 3 different mice. **(c)** Typical action potential traces of DRN-projecting DA^{VTA} neurons expressing hM4Di in

response to 10 μM CNO. (d-e) Firing frequency **(d)** and resting membrane potential **(e)** of DRN-projecting DA^{VTA} neurons in response to 10 μM CNO followed by a wash. Results are shown as individual data points. $*P < 0.05$ in one-way ANOVA analyses followed by Dunnett's post hoc test (n = 15 neurons from 3 mice per group). **(f)** Baseline body weight on the day before the ABA paradigm started. Results are shown as mean ± s.e.m. with individual data points (n = 7 mice per group).

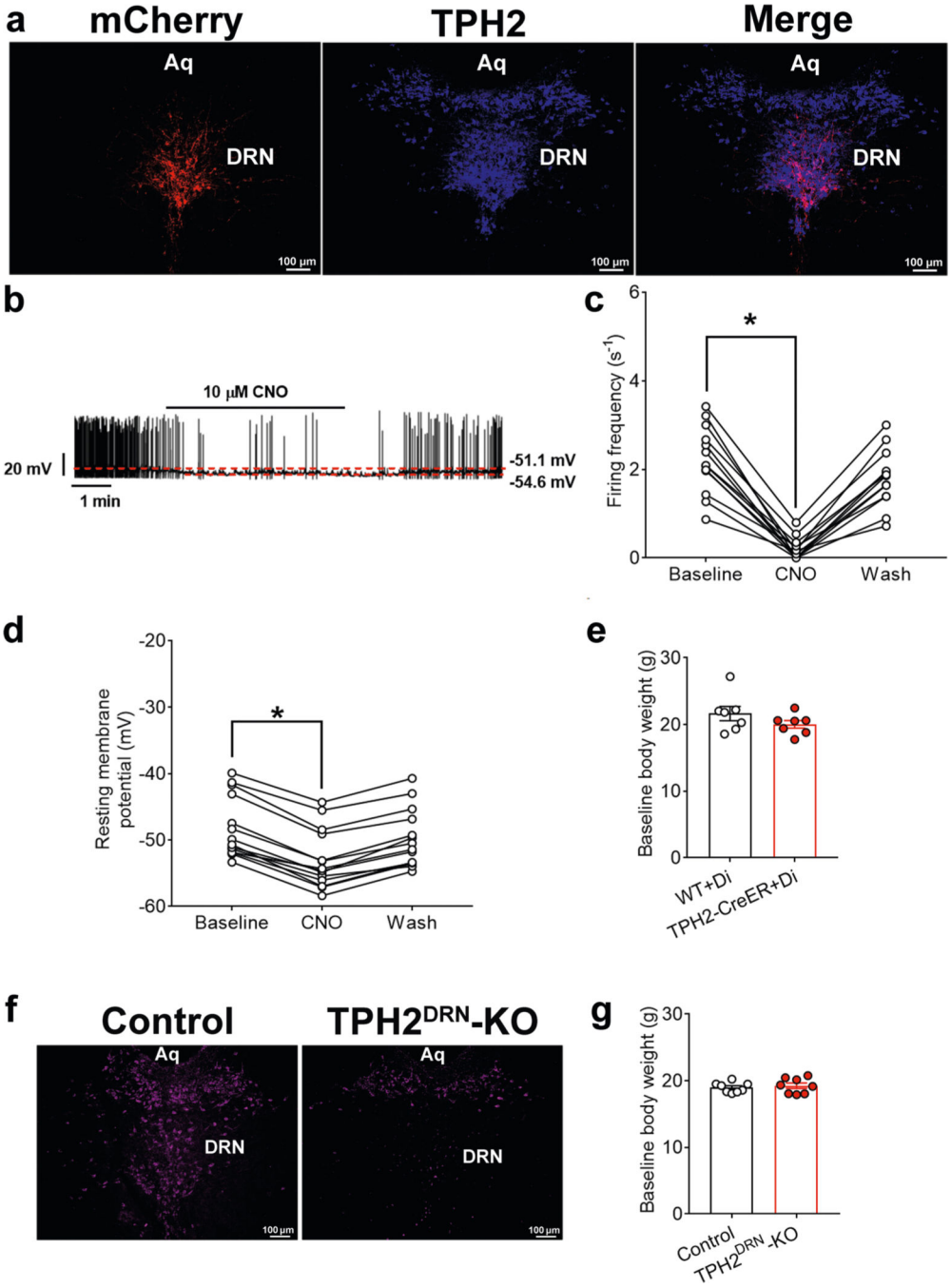

Extended Data Fig. 6 |. 5-HT^{DRN} neurons mediate activity-based anorexia.

(a) Representative microscopic images showing expression of mCherry (left), TPH2 (middle) and merge (right) in the DRN of *TPH2-CreER* mice receiving Cre-dependent AAV expressing hM4Di-mCherry in the DRN. Scale bars = 100 μm. Aq, aqueduct; DRN, dorsal Raphe nucleus. **(b)** Typical action potential traces of 5-HT^{DRN} neurons expressing hM4Di in response to 10 μM CNO. (c-d) Firing frequency **(c)** and resting membrane potential **(d)** of 5-HT^{DRN} neurons in response to 10 μM CNO followed by a wash. Results are shown as individual data points. *$P < 0.05$ in one-way ANOVA analyses followed by Dunnett's post hoc test (n = 13 neurons from 3 mice per group). **(e)** Baseline body weight on the day before the ABA paradigm started. Results are shown as mean ± s.e.m. with individual data points (n = 7 mice per group). **(f)** Representative microscopic images showing TPH2 immunoreactivity in the DRN of control and TPH2^{DRN}-KO mice. Scale bars = 100 μm. **(g)** Baseline body weight on the day before the ABA paradigm started. Results are shown as mean ± s.e.m. with individual data points (n = 8 mice per group).

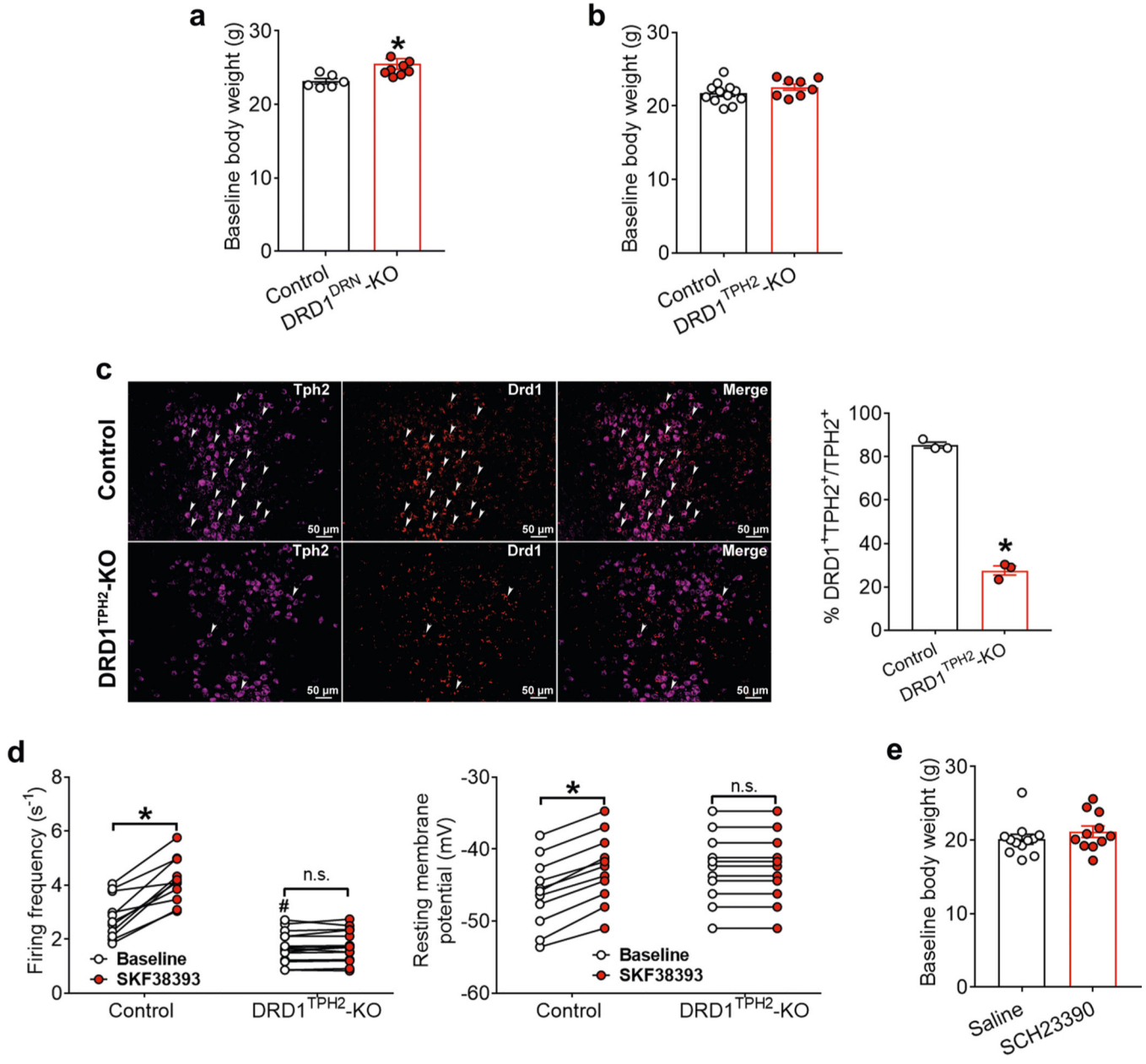

Extended Data Fig. 7 |. DRD1 in 5-HT^{DRN} neurons mediates activity-based anorexia.

(a) Baseline body weight of control or DRD1^{DRN}-KO mice on the day before the ABA paradigm started. Results are shown as mean ± s.e.m. with individual data points. *$P <$ 0.05 in two-sided unpaired t-tests (n = 6 or 9 mice per group). **(b)** Baseline body weight of control or DRD1^{TPH2}-KO mice on the day before the ABA paradigm started. Results are shown as mean ± s.e.m. with individual data points (n = 8 or 12 mice per group). **(c)** RNAscope detecting *Tph2* and *Drd1* mRNAs in the DRN of control and DRD1^{TPH2}-KO mice. Scale bars = 50 μm. Arrowheads point to double labelled neurons. Quantification of the percentage of Tph2+ neurons co-expressing Drd1 are shown as mean ± s.e.m. with individual data points. *$P <$ 0.05 in unpaired two-sided t-tests (n = 3 mice per group). **(d)** Firing frequency and resting membrane potential in 5-HT^{DRN} neurons from control or

DRD1^{TPH2}-KO mice recorded at the baseline or in response to SKF38393 (1 μM). Results are shown as individual data points. *$P < 0.05$ between baseline vs. SKF38393; # $P < 0.05$ between control vs. DRD2^{TPH2}-KO in two-way ANOVA analyses followed by Sidak's post hoc test (n = 11 or 16 neurons from 3 mice per group). **(e)** Baseline body weight of saline or SCH23390-treated mice on the day before the ABA paradigm started. Results are shown as mean ± s.e.m. with individual data points (n = 11 or 12 mice per group).

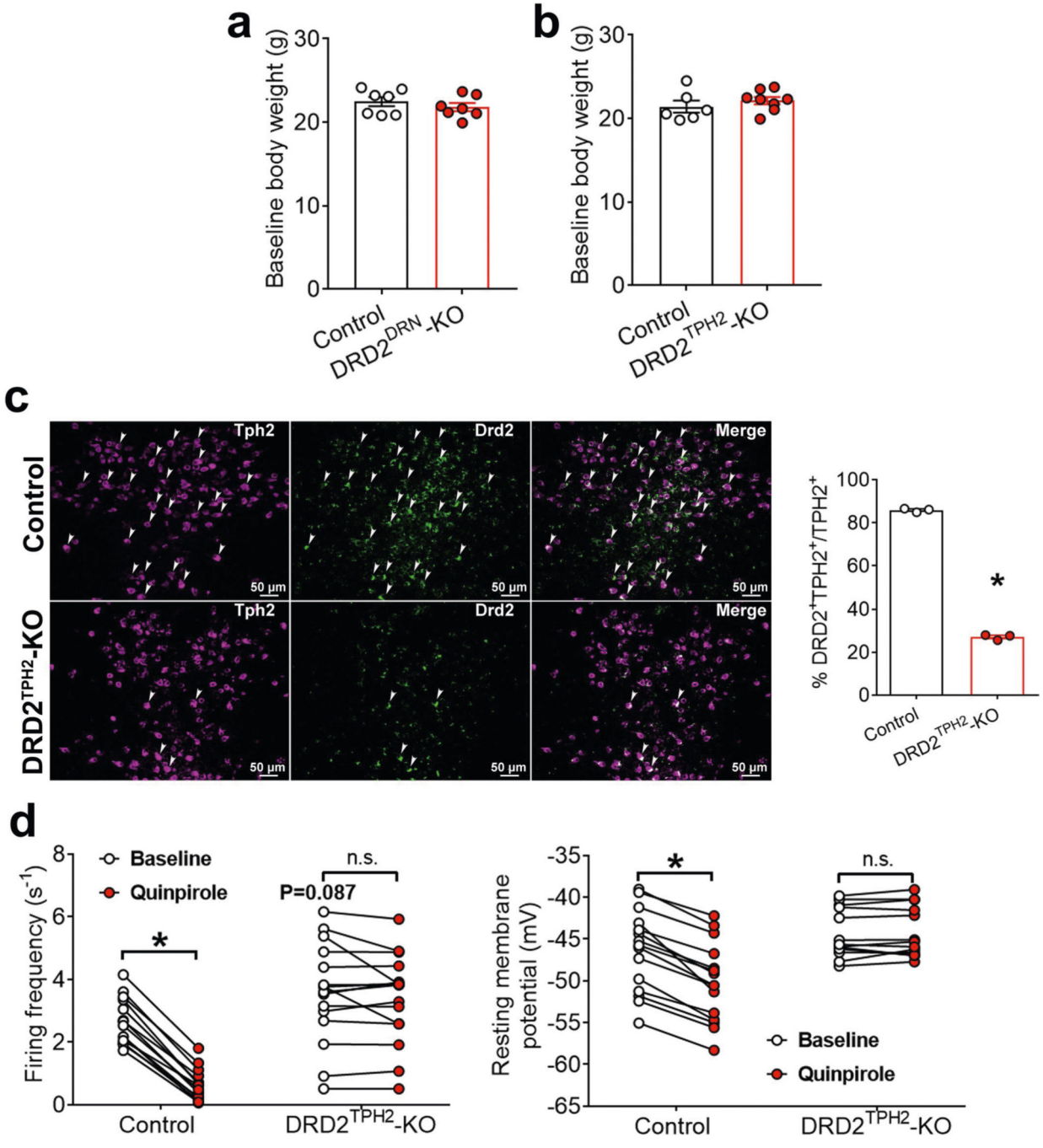

Extended Data Fig. 8 |. DRD2 prevents anorexia and weight loss during hyperactivity.

(a) Baseline body weight of control or DRD2^{DRN}-KO mice on the day before the ABA paradigm started. Results are shown as mean ± s.e.m. with individual data points (n = 7 mice per group). **(b)** Baseline body weight of control or DRD2^{TPH2}-KO mice on the day before the ABA paradigm started. Results are shown as mean ± s.e.m. with individual data points (n = 6 or 8 mice per group). **(c)** RNAscope detecting *Tph2* and *Drd2* mRNAs in the DRN of control and DRD2^{TPH2}-KO mice. Scale bars = 50 μm. Arrowheads point to double labelled neurons. Quantification of the percentage of Tph2+ neurons co-expressing Drd2 are shown as mean ± s.e.m. with individual data points. *$P < 0.05$ in unpaired two-sided t-tests (n = 3 mice per group). **(d)** Firing frequency and resting membrane potential in 5-HT^{DRN} neurons from control or DRD2^{TPH2}-KO mice recorded at the baseline or in response to quinpirole (1 μM). Results are shown as individual data points. *$P < 0.05$ between baseline vs. quinpirole; $P = 0.087$ between the baseline of control vs. the baseline of DRD2^{TPH2}-KO in two-way ANOVA analyses followed by Sidak's post hoc test (n = 13 or 15 neurons from 3 mice per group).

Supplementary Material

Refer to Web version on PubMed Central for supplementary material.

Acknowledgements

The investigators were supported by the following grants from the National Institutes of Health: R01DK114279, R01DK109934 and R21NS108091 to Q.T.; R00 DK107008, R01 DK123098 and P30 DK020595 to P.X.; K01DK119471 to C.W.; R01DK109194 and R56DK109194 to Q.W.; P01DK113954, R01DK115761 and R01DK117281 to Y.X.; R01DK120858 to Q.T. and Y.X.; and P20 GM135002 to Y.H. The investigators were also supported by the US Department of Defense (Innovative Grant W81XWH-19-PRMRP-DA to P.X.), Pew Charitable Trust awards (0026188) to Q.W., Baylor Collaborative Faculty Research Investment Program grants to Q.W., USDA/CRIS (51000-064-01S to Y.X. and Q.W.) and the American Diabetes Association (7-13-JF-61 to Q.W., 1-17-PDF-138 to Y.H. and 1-15-BS-184 to Q.T.). The Ad-iN/WED virus was kindly provided by M. Myers (University of Michigan).

Data availability

All data generated or analyzed during this study are included in the published article (and its supplementary information files). Additional data that support the findings of this study are available upon reasonable request from the corresponding authors (Yanlin He and Y.X.). Source data are provided with this paper.

References

1. Papadopoulos FC, Ekbom A, Brandt L. & Ekselius L. Excess mortality, causes of death and prognostic factors in anorexia nervosa. Br. J. Psychiatry 194, 10–17 (2009). [PubMed: 19118319]
2. Watson HJ et al. Genome-wide association study identifies eight risk loci and implicates metabo-psychiatric origins for anorexia nervosa. Nat. Genet. 51, 1207–1214 (2019). [PubMed: 31308545]
3. Tsai HC et al. Phasic firing in dopaminergic neurons is sufficient for behavioral conditioning. Science 324, 1080–1084 (2009). [PubMed: 19389999]
4. Zhou QY & Palmiter RD Dopamine-deficient mice are severely hypoactive, adipsic, and aphagic. Cell 83, 1197–1209 (1995). [PubMed: 8548806]
5. Paladini CA & Roeper J. Generating bursts (and pauses) in the dopamine midbrain neurons. Neuroscience 282, 109–121 (2014). [PubMed: 25073045]

6. Richfield EK, Penney JB & Young AB Anatomical and affinity state comparisons between dopamine D1 and D2 receptors in the rat central nervous system. Neuroscience 30, 767–777 (1989). [PubMed: 2528080]
7. Bergen AW et al. Association of multiple DRD2 polymorphisms with anorexia nervosa. Neuropsychopharmacology 30, 1703–1710 (2005). [PubMed: 15920508]
8. Peng S. et al. Dopamine receptor D2 and catechol-O-methyltransferase gene polymorphisms associated with anorexia nervosa in Chinese Han population: DRD2 and COMT gene polymorphisms were associated with AN. Neurosci. Lett. 616, 147–151 (2016). [PubMed: 26808641]
9. Nisoli E. et al. D2 dopamine receptor (DRD2) gene Taq1A polymorphism and the eating-related psychological traits in eating disorders (anorexia nervosa and bulimia) and obesity. Eat. Weight Disord. 12, 91–96 (2007). [PubMed: 17615493]
10. Frieling H. et al. Epigenetic dysregulation of dopaminergic genes in eating disorders. Int. J. Eat. Disord. 43, 577–583 (2010). [PubMed: 19728374]
11. Gervasini G. et al. Influence of dopamine polymorphisms on the risk for anorexia nervosa and associated psychopathological features. J. Clin. Psychopharmacol. 33, 551–555 (2013). [PubMed: 23775054]
12. Walton E. et al. Exploration of shared genetic architecture between subcortical brain volumes and anorexia nervosa. Mol. Neurobiol. 56, 5146–5156 (2019). [PubMed: 30519816]
13. Barbato G, Fichele M, Senatore I, Casiello M. & Muscettola G. Increased dopaminergic activity in restricting-type anorexia nervosa. Psychiatry Res. 142, 253–255 (2006). [PubMed: 16626809]
14. Kaye WH, Frank GK & McConaha C. Altered dopamine activity after recovery from restricting-type anorexia nervosa. Neuropsychopharmacology 21, 503–506 (1999). [PubMed: 10481833]
15. Lechin F, van der Dijs B. & Hernandez-Adrian G. Dorsal raphe vs. median raphe serotonergic antagonism. Anatomical, physiological, behavioral, neuroendocrinological, neuropharmacological and clinical evidences: relevance for neuropharmacological therapy. Prog. Neuropsychopharmacol. Biol. Psychiatry 30, 565–585 (2006). [PubMed: 16436311]
16. He Y. et al. 5-HT recruits distinct neurocircuits to inhibit hunger-driven and non-hunger-driven feeding. Mol. Psychiatry 26, 7211–7224 (2021). [PubMed: 34290371]
17. McGuirk J, Goodall E, Silverstone T. & Willner P. Differential effects of d-fenfluramine, l-fenfluramine and d-amphetamine on the microstructure of human eating behaviour. Behav. Pharm. 2, 113–119 (1991).
18. Xu P. et al. Activation of serotonin 2C receptors in dopamine neurons inhibits binge-like eating in mice. Biol. Psychiatry 81, 737–747 (2017). [PubMed: 27516377]
19. Saller CF & Stricker EM Hyperphagia and increased growth in rats after intraventricular injection of 5,7-dihydroxytryptamine. Science 192, 385–387 (1976). [PubMed: 1257774]
20. Kaye WH, Gwirtsman HE, George DT & Ebert MH Altered serotonin activity in anorexia nervosa after long-term weight restoration. Does elevated cerebrospinal fluid 5-hydroxyindoleacetic acid level correlate with rigid and obsessive behavior? Arch. Gen. Psychiatry 48, 556–562 (1991). [PubMed: 1710099]
21. Bailer UF et al. Exaggerated 5-HT1A but normal 5-HT2A receptor activity in individuals ill with anorexia nervosa. Biol. Psychiatry 61, 1090–1099 (2007). [PubMed: 17241616]
22. Galusca B. et al. Organic background of restrictive-type anorexia nervosa suggested by increased serotonin 1A receptor binding in right frontotemporal cortex of both lean and recovered patients: [18F]MPPF PET scan study. Biol. Psychiatry 64, 1009–1013 (2008). [PubMed: 18639866]
23. Frank GK & Kaye WH Positron emission tomography studies in eating disorders: multireceptor brain imaging, correlates with behavior and implications for pharmacotherapy. Nucl. Med. Biol. 32, 755–761 (2005). [PubMed: 16243652]
24. Bailer UF et al. Interaction between serotonin transporter and dopamine D2/D3 receptor radioligand measures is associated with harm avoidant symptoms in anorexia and bulimia nervosa. Psychiatry Res. 211, 160–168 (2013). [PubMed: 23154100]
25. Ogawa SK, Cohen JY, Hwang D, Uchida N. & Watabe-Uchida M. Organization of monosynaptic inputs to the serotonin and dopamine neuromodulatory systems. Cell Rep. 8, 1105–1118 (2014). [PubMed: 25108805]

26. Ogawa SK & Watabe-Uchida M. Organization of dopamine and serotonin system: anatomical and functional mapping of monosynaptic inputs using rabies virus. Pharmacol. Biochem. Behav. 174, 9–22 (2018). [PubMed: 28476484]
27. Li Y. et al. Rostral and caudal ventral tegmental area GABAergic inputs to different dorsal raphe neurons participate in opioid dependence. Neuron 101, 748–761 (2019). [PubMed: 30638902]
28. Pollak Dorocic I. et al. A whole-brain atlas of inputs to serotonergic neurons of the dorsal and median raphe nuclei. Neuron 83, 663–678 (2014). [PubMed: 25102561]
29. Matthews GA et al. Dorsal raphe dopamine neurons represent the experience of social isolation. Cell 164, 617–631 (2016). [PubMed: 26871628]
30. Leinninger GM et al. Leptin action via neurotensin neurons controls orexin, the mesolimbic dopamine system and energy balance. Cell Metab. 14, 313–323 (2011). [PubMed: 21907138]
31. Fink KB & Gothert M. 5-HT receptor regulation of neurotransmitter release. Pharm. Rev. 59, 360–417 (2007). [PubMed: 18160701]
32. Szczypka MS et al. Dopamine production in the caudate putamen restores feeding in dopamine-deficient mice. Neuron 30, 819–828 (2001). [PubMed: 11430814]
33. Mequinion M, Chauveau C. & Viltart O. The use of animal models to decipher physiological and neurobiological alterations of anorexia nervosa patients. Front. Endocrinol. (Lausanne) 6, 68 (2015). [PubMed: 26042085]
34. Lerner TN et al. Intact-brain analyses reveal distinct information carried by SNc dopamine subcircuits. Cell 162, 635–647 (2015). [PubMed: 26232229]
35. Nectow AR et al. Identification of a brainstem circuit controlling feeding. Cell 170, 429–442 (2017). [PubMed: 28753423]
36. Hall JF & Hanford PV Activity as a function of a restricted feeding schedule. J. Comp. Physiol. Psychol. 47, 362–363 (1954). [PubMed: 13221681]
37. Boakes RA, Mills KJ & Single JP Sex differences in the relationship between activity and weight loss in the rat. Behav. Neurosci. 113, 1080–1089 (1999). [PubMed: 10571490]
38. Attia E. Anorexia nervosa: current status and future directions. Annu. Rev. Med. 61, 425–435 (2010). [PubMed: 19719398]
39. Floresco SB, West AR, Ash B, Moore H. & Grace AA Afferent modulation of dopamine neuron firing differentially regulates tonic and phasic dopamine transmission. Nat. Neurosci. 6, 968–973 (2003). [PubMed: 12897785]
40. Grieder TE et al. Phasic D1 and tonic D2 dopamine receptor signaling double dissociate the motivational effects of acute nicotine and chronic nicotine withdrawal. Proc. Natl Acad. Sci. USA 109, 3101–3106 (2012). [PubMed: 22308372]
41. Chaudhury D. et al. Rapid regulation of depression-related behaviours by control of midbrain dopamine neurons. Nature 493, 532–536 (2013). [PubMed: 23235832]
42. Frank GK et al. The partial dopamine D2 receptor agonist aripiprazole is associated with weight gain in adolescent anorexia nervosa. Int. J. Eat. Disord. 50, 447–450 (2017). [PubMed: 28334444]
43. Frank GKW Pharmacotherapeutic strategies for the treatment of anorexia nervosa—too much for one drug? Expert Opin. Pharmacother. 21, 1045–1058 (2020). [PubMed: 32281881]
44. Klenotich SJ, Ho EV, McMurray MS, Server CH & Dulawa SC Dopamine D2/3 receptor antagonism reduces activity-based anorexia. Transl. Psychiatry 5, e613 (2015). [PubMed: 26241351]
45. Bello EP et al. Cocaine supersensitivity and enhanced motivation for reward in mice lacking dopamine D2 autoreceptors. Nat. Neurosci. 14, 1033–1038 (2011). [PubMed: 21743470]
46. White W, Beyer JD & White IM Acute withdrawal-related hypophagia elicited by amphetamine is attenuated by pretreatment with selective dopamine D1 or D2 receptor antagonists in rats. Physiol. Behav. 151, 345–354 (2015). [PubMed: 26256519]
47. Szczypka MS et al. Feeding behavior in dopamine-deficient mice. Proc. Natl Acad. Sci. USA 96, 12138–12143 (1999). [PubMed: 10518589]
48. Qu N. et al. A POMC-originated circuit regulates stress-induced hypophagia, depression, and anhedonia. Mol. Psychiatry 25, 1006–1021 (2019). [PubMed: 31485012]

49. Boekhoudt L. et al. Does activation of midbrain dopamine neurons promote or reduce feeding? Int J. Obes. (Lond.) 41, 1131–1140 (2017). [PubMed: 28321131]
50. Han Y. et al. A hindbrain dopaminergic neural circuit prevents weight gain by reinforcing food satiation. Sci. Adv. 7, eabf8719 (2021).
51. Zhu X, Ottenheimer D. & DiLeone RJ Activity of D1/2 receptor expressing neurons in the nucleus accumbens regulates running, locomotion, and food intake. Front. Behav. Neurosci. 10, 66 (2016). [PubMed: 27147989]
52. Welch AC et al. Dopamine D2 receptor overexpression in the nucleus accumbens core induces robust weight loss during scheduled fasting selectively in female mice. Mol. Psychiatry 26, 3765–3777 (2019). [PubMed: 31863019]
53. Land BB et al. Medial prefrontal D1 dopamine neurons control food intake. Nat. Neurosci. 17, 248–253 (2014). [PubMed: 24441680]
54. Denis RGP et al. Palatability can drive feeding independent of AgRP neurons. Cell Metab. 25, 975 (2017). [PubMed: 28380385]
55. Madisen L. et al. A robust and high-throughput Cre reporting and characterization system for the whole mouse brain. Nat. Neurosci. 13, 133–140 (2010). [PubMed: 20023653]
56. Sarinana J, Kitamura T, Kunzler P, Sultzman L. & Tonegawa S. Differential roles of the dopamine 1-class receptors, D1R and D5R, in hippocampal dependent memory. Proc. Natl Acad. Sci. USA 111, 8245–8250 (2014). [PubMed: 24843151]
57. Carlson KS, Whitney MS, Gadziola MA, Deneris ES & Wesson DW Preservation of essential odor-guided behaviors and odor-based reversal learning after targeting adult brain serotonin synthesis. eNeuro 3, ENEURO.0257–16.2016 (2016).
58. He Y. et al. A small potassium current in AgRP/NPY neurons regulates feeding behavior and energy metabolism. Cell Rep. 17, 1807–1818 (2016). [PubMed: 27829152]
59. Atasoy D, Betley JN, Su HH & Sternson SM Deconstruction of a neural circuit for hunger. Nature 488, 172–177 (2012). [PubMed: 22801496]
60. Kurokawa K, Mizuno K. & Ohkuma S. Dopamine D1 receptor signaling system regulates ryanodine receptor expression in ethanol physical dependence. Alcohol Clin. Exp. Res. 37, 771–783 (2013). [PubMed: 23278119]
61. Sutoo D. & Akiyama K. Effect of dopamine receptor anatagonists on the calcium-dependent central function that reduces blood pressure in spontaneously hypertensive rats. Neurosci. Lett. 269, 133–136 (1999). [PubMed: 10454150]
62. Pardo M. et al. Peripheral leptin and ghrelin receptors are regulated in a tissue-specific manner in activity-based anorexia. Peptides 31, 1912–1919 (2010). [PubMed: 20600421]
63. Galassetti P. et al. Effect of sex on counterregulatory responses to exercise after antecedent hypoglycemia in type 1 diabetes. Am. J. Physiol. Endocrinol. Metab. 287, E16–E24 (2004). [PubMed: 14998785]
64. Dubreucq S. et al. Ventral tegmental area cannabinoid type-1 receptors control voluntary exercise performance. Biol. Psychiatry 73, 895–903 (2013). [PubMed: 23237313]
65. Aragona BJ et al. Nucleus accumbens dopamine differentially mediates the formation and maintenance of monogamous pair bonds. Nat. Neurosci. 9, 133–139 (2006). [PubMed: 16327783]
66. Atasoy D, Aponte Y, Su HH & Sternson SM A FLEX switch targets channelrhodopsin-2 to multiple cell types for imaging and long-range circuit mapping. J. Neurosci. 28, 7025–7030 (2008). [PubMed: 18614669]
67. Petreanu L, Huber D, Sobczyk A. & Svoboda K. Channelrhodopsin-2-assisted circuit mapping of long-range callosal projections. Nat. Neurosci. 10, 663–668 (2007). [PubMed: 17435752]
68. Li C. et al. Defined paraventricular hypothalamic populations exhibit differential responses to food contingent on caloric state. Cell Metab. 29, 681–694 (2018). [PubMed: 30472090]
69. Li Y. et al. Serotonin neurons in the dorsal raphe nucleus encode reward signals. Nat. Commun. 7, 10503 (2016). [PubMed: 26818705]
70. Fu Y. et al. Gut hormone GIP induces inflammation and insulin resistance in the hypothalamus. Endocrinology 161, bqaa102 (2020).

71. Sakata S. et al. Autosomal recessive complete STAT1 deficiency caused by compound heterozygous intronic mutations. Int. Immunol. 30, 663–671 (2020).

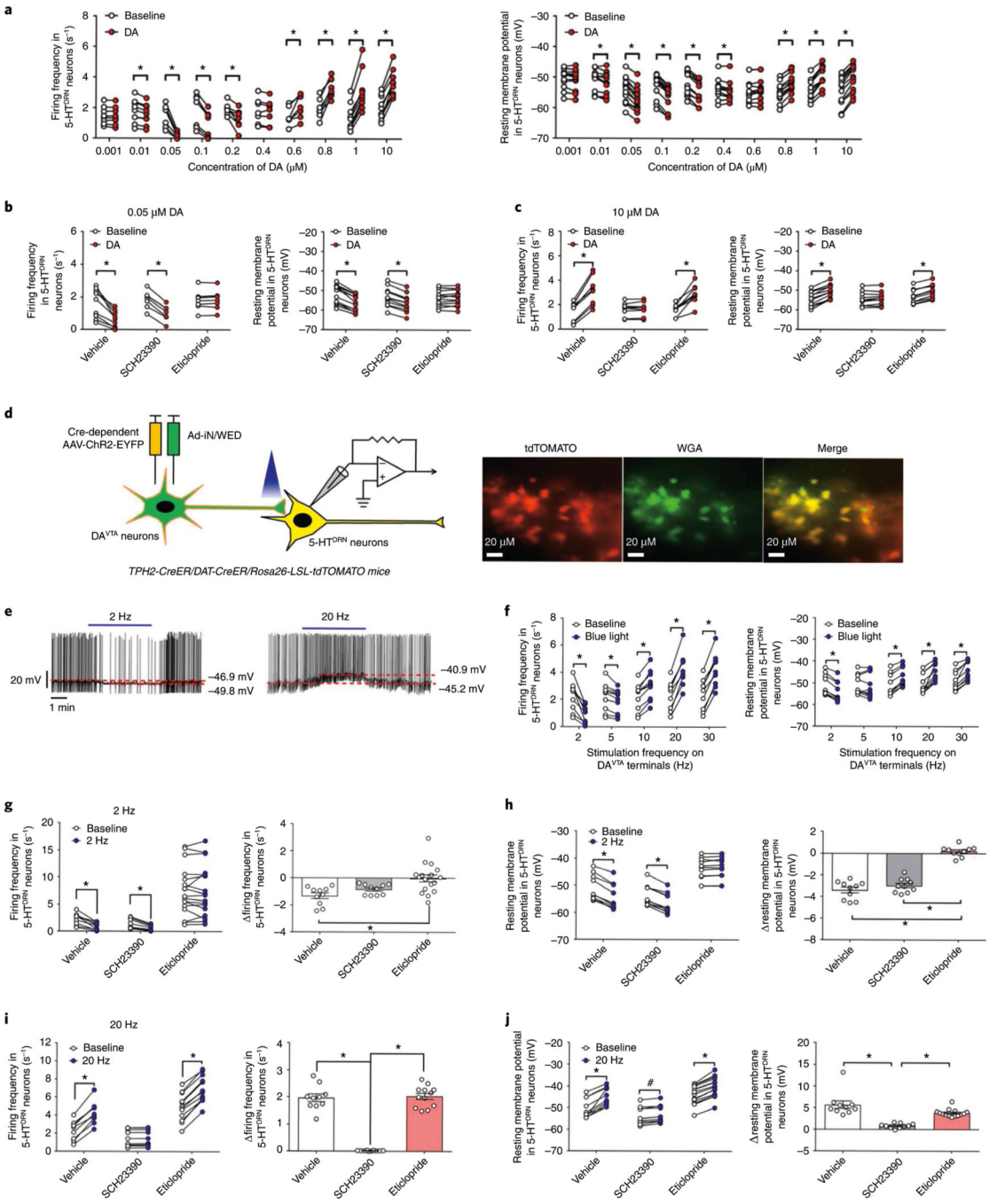

Fig. 1 |. Bidirectional regulations of DA^{VTA} neurons on 5-HT^{DRN} neurons.

a, Firing frequency and resting membrane potential of 5-HT^{DRN} neurons. Results are shown as individual data points. *$P < 0.05$ between baseline versus DA treatment in two-sided paired *t*-tests ($n = 7$ or 14 neurons from three mice). **b**, **c**, Firing frequency and resting membrane potential in response to 0.05 μM (**b**) or 10 μM (**c**) DA. Results are shown as individual data points. *$P < 0.05$ in two-sided *t*-tests. $n = 7$ or 13 neurons from three mice in **b** and $n = 9$ or 13 neurons from three mice in **c**. **d**, Recordings in 5-HT^{DRN} neurons in response to photostimulation of DA^{VTA}-originated fibers. Right panel: representative

images showing a DRN neuron labeled by tdTOMATO and WGA (repeated in three mice). **e**, Typical action potential traces of 5-HT^{DRN} neurons in response to photostimulation. **f**, Firing frequency and resting membrane potential of 5-HT^{DRN} neurons in response to photostimulation. Results are shown as individual data points. *$P < 0.05$ between blue light versus baseline in two-sided paired *t*-tests ($n = 10$ neurons from three mice). **g**, **h**, Left panels: firing frequency (**g**) and resting membrane potential (**h**) in response to 2-Hz stimulation. Results are shown as individual data points. *$P < 0.05$ in two-way ANOVA followed by Sidak's test ($n = 10$ neurons from three mice). Right panels: changes in firing frequency (**g**) and resting membrane potential (**h**) calculated from data in the left panels. Results are shown as mean ± s.e.m. with individual data points. *$P < 0.05$ in one-way ANOVA followed by Tukey's tests ($n = 10$ neurons from three mice). **i**, **j**, Left panels: firing frequency (**i**) and resting membrane potential (**j**) in response to 20-Hz stimulation. Results are shown as individual data points. *$P < 0.05$ in two-way ANOVA followed by Sidak's test; #$P < 0.05$ in two-sided paired *t*-test ($n = 10$ or 14 neurons from three mice). Right panels: changes in firing frequency (**i**) and resting membrane potential (**j**) calculated from data in the left panels. Results are shown as mean ± s.e.m. with individual data points. *$P < 0.05$ in one-way ANOVA followed by Tukey's tests ($n = 10$ or 14 neurons from three mice). Detailed statistics information is in the Source Data file.

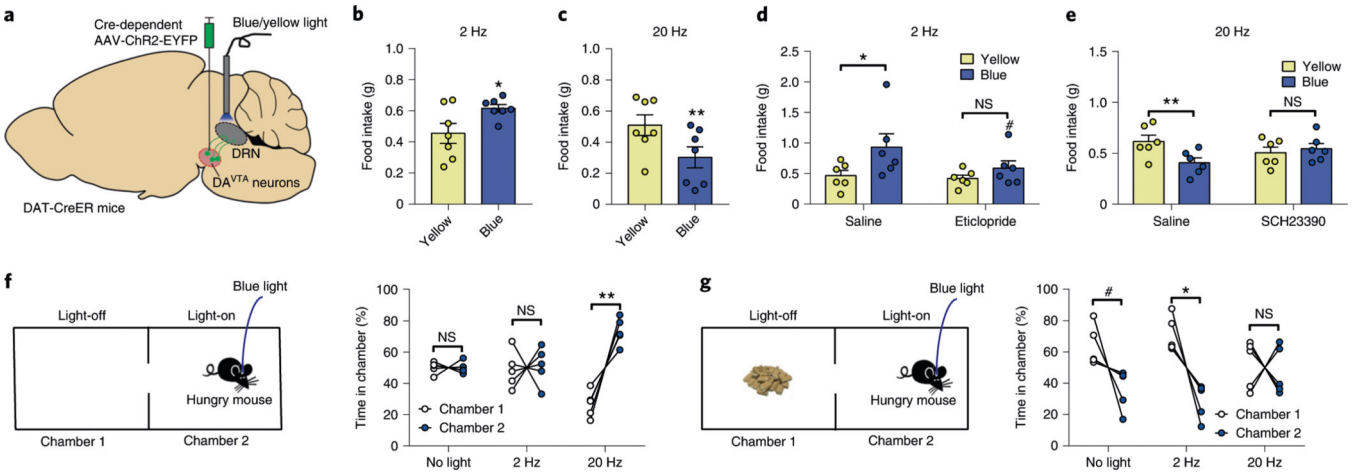

Fig. 2 |. Bidirectional effects of the DA^{VTA}→DRN circuit on feeding.

a, Schematic experimental strategy using the Cre-dependent AAV-expressing ChR2-EYFP to activate the DA^{VTA}→DRN projections. **b**, **c**, Mice were fasted overnight; 1-hour refeeding was measured next morning; and photostimulation, yellow or blue at 2 Hz (**b**) or 20 Hz (**c**), was performed during refeeding. Results are shown as mean ± s.e.m. with individual data points. *$P < 0.05$ or **$P < 0.01$ in two-sided paired t-tests ($n = 7$ mice per group). **d**, Effects of 2-Hz photostimulation (yellow or blue) on refeeding in hungry mice with pre-injections of saline or 100 ng of eticlopride into the DRN 1 hour before refeeding. Results are shown as individual data points. *$P < 0.05$ between yellow and blue; #$P < 0.05$ between saline and eticlopride in two-sided paired t-tests ($n = 6$ mice per group). **e**, Effects of 20-Hz photostimulation (yellow or blue) on refeeding in hungry mice with pre-injections of saline or 10 ng of SCH23390 into the DRN 1 hour before refeeding. Results are shown as individual data points. **$P < 0.01$ in two-sided paired t-tests ($n = 6$ mice per group). **f**, Left: the experimental paradigm to measure real-time place preference in hungry mice with the DA^{VTA}→DRN projections unstimulated when in chamber 1 and activated when in chamber 2; right: the percentage of time spent in each chamber in mice with or without blue light stimulation (2 Hz or 20 Hz) coupled to chamber 2. Results are shown as individual data points. **$P < 0.01$ in two-sided paired t-tests ($n = 5$ mice per group). **g**, Left: the experimental paradigm to measure real-time place preference in hungry mice with the DA^{VTA}→DRN projections unstimulated when in food-containing chamber 1 and activated when in chamber 2; right: the percentage of time spent in each chamber in mice with or without blue light stimulation (2 Hz or 20 Hz) coupled to chamber 2. Results are shown as individual data points. #$P < 0.05$ in two-sided unpaired t-tests; *$P < 0.05$ in two-sided paired t-tests ($n = 5$ mice per group). Detailed statistics information is in the Source Data file. NS, not significant.

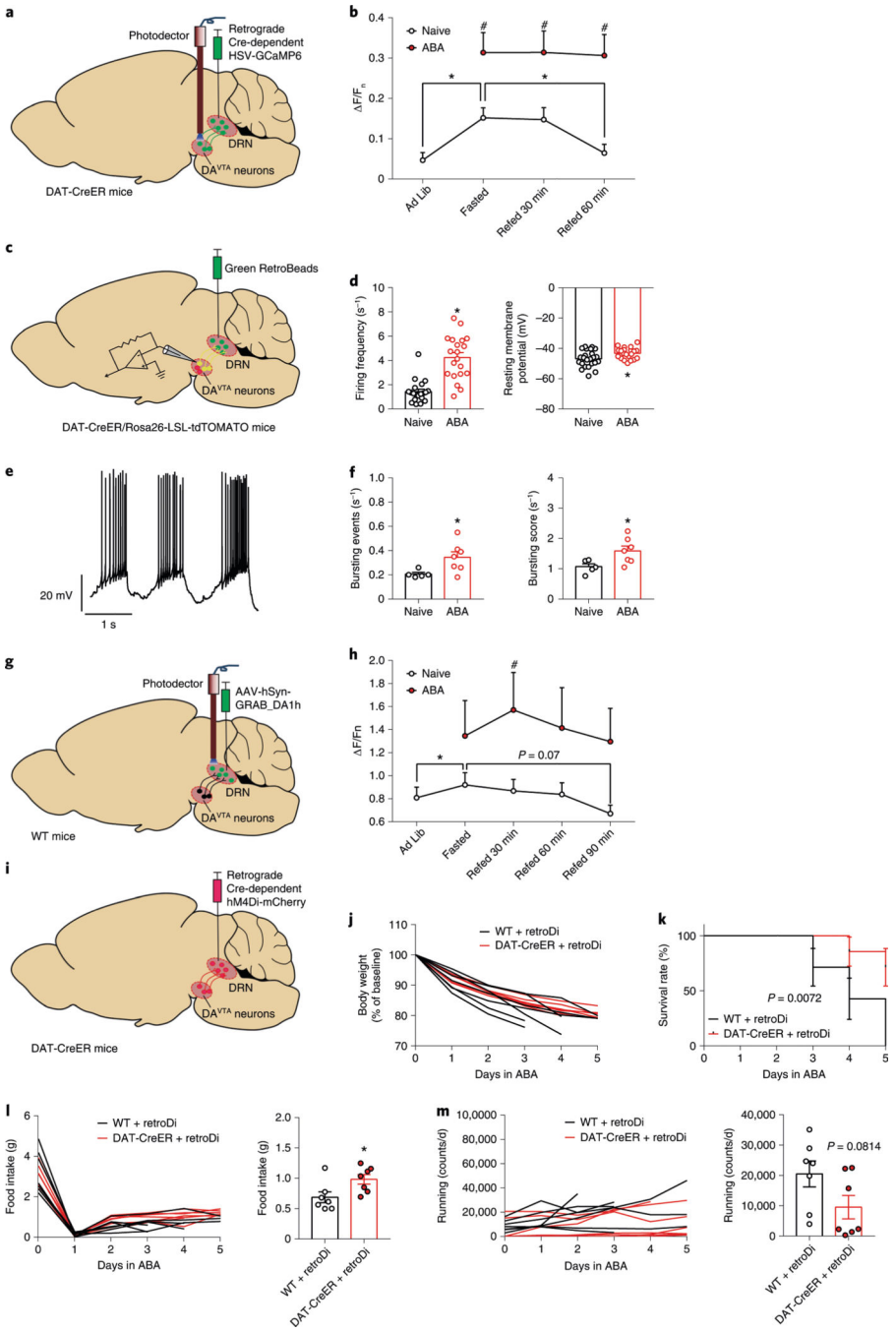

Fig. 3 |. DRN-projecting DA^{VTA} neurons mediate activity-based anorexia.

a, Using retrograde Cre-dependent HSV-GCaMP6 to monitor the DRN-projecting DA^{VTA} neurons. **b**, DRN-projecting DA^{VTA} neuron activity in naive mice or in ABA mice. Results are shown as mean ± s.e.m. *$P < 0.05$ among different time points in naive mice; #$P < 0.05$ between naive mice and ABA mice at the same time point in two-sided unpaired *t*-tests (n = 5 mice). **c**, Using Green RetroBeads to record activity of DRN-projecting DA^{VTA} neurons. **d**, Tonic firing frequency and resting membrane potential at fasted condition. Results are shown as mean ± s.e.m. with individual data points. *$P < 0.05$ in two-sided unpaired *t*-tests

(*n* = 20 or 24 neurons from three mice). **e**, Typical action potential traces showing bursting events. **f**, Bursting event frequency and bursting score at fasted condition. Results are shown as mean ± s.e.m. with individual data points. **P* < 0.05 in two-sided unpaired *t*-tests (*n* = 5 or 7 neurons from three mice). **g**, Using an AAV-hSyn-GRAB_DA1h to monitor the DA levels in the DRN. **h**, DA levels in the DRN in naive mice or in ABA mice. Results are shown as mean ± s.e.m. **P* < 0.05 among different time points in naive mice in two-sided paired *t*-tests; #*P* < 0.05 between naive mice and ABA mice at the same time point in two-sided paired *t*-tests (*n* = 5 mice). **i**, Using a retrograde Cre-dependent AAV-hM4Di-mCherry to inhibit DRN-projecting DA^{VTA} neurons. **j**, Body weight change (% of the baseline). Results are shown as individual data lines. Mice were euthanized once they lost more than 20% of body weight. **k**, Survival rate. *P* = 0.0072 in log-rank (Mantel–Cox) test (*n* = 7 mice per group). **l**, Left panel: daily food intake of each individual mouse; right panel: daily food intake during days 2–5. Results are shown as mean ± s.e.m. with individual data points. **P* < 0.05 in two-sided unpaired *t*-tests (*n* = 7 mice per group). **m**, Left panel: daily running wheel activity of each individual mouse; right panel: daily running wheel activity during days 2–5. Results are shown as mean ± s.e.m. with individual data points. *P* values are indicated in two-sided unpaired *t*-tests (*n* = 7 mice). Detailed statistics information is in the Source Data file. WT, wild-type.

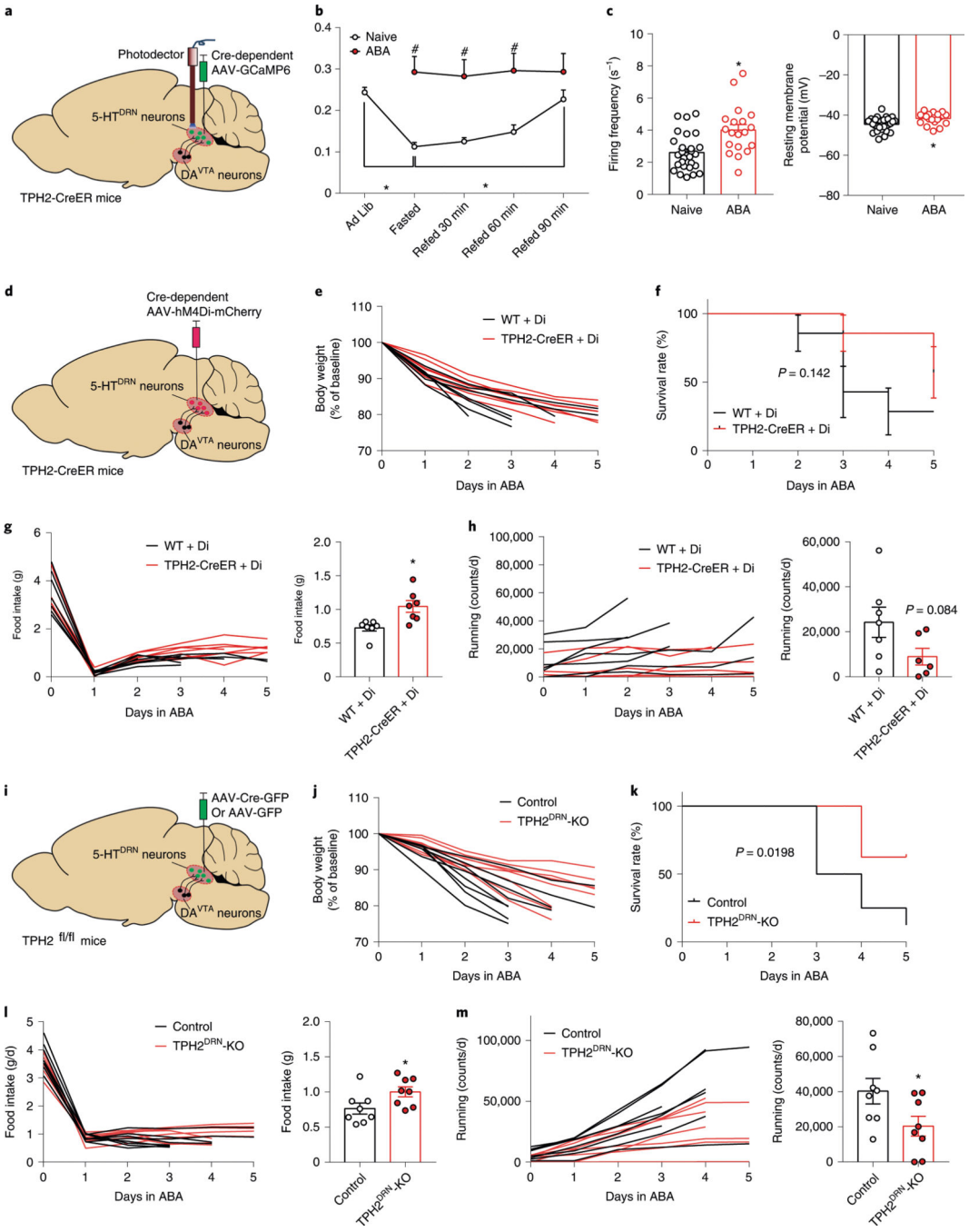

Fig. 4 |. 5-HT^{DRN} neurons mediate activity-based anorexia.

a, Using Cre-dependent AAV-GCaMP6 to monitor the 5-HT^{DRN} neuron activity. **b**, 5-HT^{DRN} neuron activity in naive mice or in ABA mice. Results are shown as mean ± s.e.m. *$P < 0.05$ among different time points in naive mice in two-sided paired t-tests; #$P < 0.05$ between naive mice and ABA mice at the same time point in two-sided paired t-tests ($n = 6$ mice). **c**, Firing frequency and resting membrane potential of 5-HT^{DRN} neurons at fasted condition. Results are shown as mean ± s.e.m. with individual data points. *$P < 0.05$ in two-sided unpaired t-tests ($n = 19$ or 28 neurons from three mice). **d**, Using a

Cre-dependent AAV-hM4Di-mCherry to inhibit 5-HT^{DRN} neurons. **e**, Body weight change (% of the baseline). Results are shown as individual data lines. Mice were euthanized once they lost more than 20% of body weight. **f**, Survival rate. $P = 0.142$ in log-rank (Mantel–Cox) test ($n = 7$ mice per group). **g**, Left panel: daily food intake of each individual mouse; right panel: daily food intake during days 2–5. Results are shown as mean ± s.e.m. with individual data points. $^*P < 0.05$ in two-sided unpaired *t*-tests ($n = 7$ mice). **h**, Left panel: daily running wheel activity of each individual mouse; right panel: daily running wheel activity during days 2–5. Results are shown as mean ± s.e.m. with individual data points. *P* values are indicated in two-sided unpaired *t*-tests ($n = 7$ mice). **i**, Mice lacking TPH2 in the DRN and their controls. **j**, Body weight change (% of the baseline). Results are shown as individual data lines. Mice were euthanized once they lost more than 20% of body weight. **k**, Survival rate. $P = 0.0198$ in log-rank (Mantel–Cox) test ($n = 8$ mice per group). **l**, Left panel: daily food intake of each individual mouse; right panel: daily food intake during days 2–5. Results are shown as mean ± s.e.m. with individual data points. $^*P < 0.05$ in two-sided unpaired *t*-tests ($n = 8$ mice). **m**, Left panel: daily running wheel activity of each individual mouse; right panel: daily running wheel activity during days 2–5. Results are shown as mean ± s.e.m. with individual data points. $^*P < 0.05$ in two-sided unpaired *t*-tests ($n = 8$ mice). Detailed statistics information is in the Source Data file.

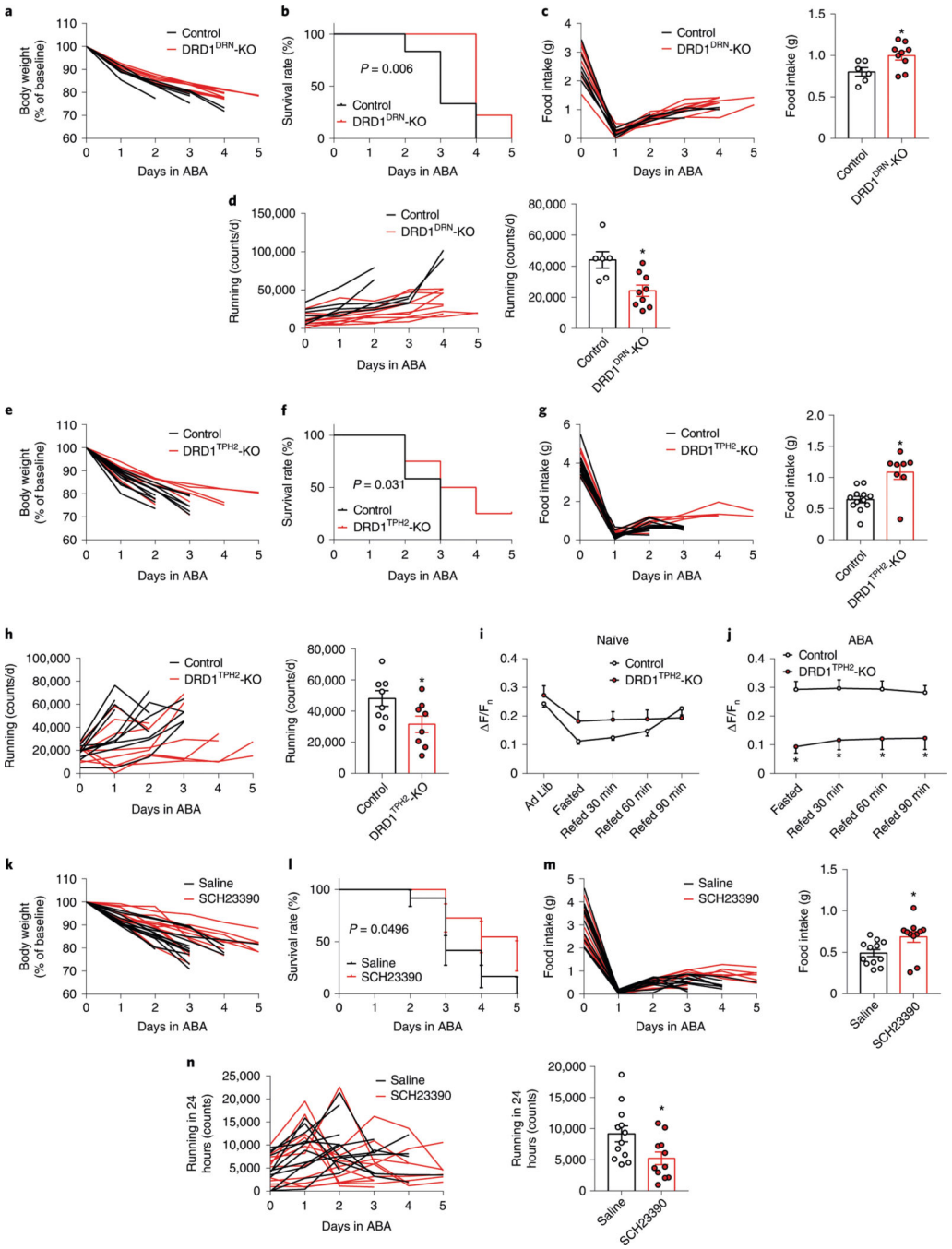

Fig. 5 |. DRD1 in 5-HT^{DRN} neurons mediates activity-based anorexia.

a, Body weight change (% of the baseline shown as individual data). Mice were euthanized once they lost more than 20% of body weight. **b**, Survival rate. $P = 0.006$ in log-rank (Mantel–Cox) test. **c**, Left panel: daily food intake of each individual mouse; right panel: daily food intake during days 2–5. Results are shown as mean ± s.e.m. with individual data points. *$P < 0.05$ in two-sided unpaired *t*-tests. **d**, Left panel: daily running wheel activity of each individual mouse; right panel: daily running wheel activity during days 2–5. Results are shown as mean ± s.e.m. with individual data points. *$P < 0.05$ in two-sided unpaired *t*-tests.

n = 6 or 9 mice in **a**–**d**. **e**, Body weight change. Results are shown as individual data lines. **f**, Survival rate. $P = 0.031$ in log-rank (Mantel–Cox) test. **g**, Left panel: daily food intake of each individual mouse; right panel: daily food intake during days 2–5. Results are shown as mean ± s.e.m. with individual data points. $^{*}P < 0.05$ in two-sided unpaired *t*-tests. **h**, Left panel: daily running wheel activity of each individual mouse; right panel: daily running wheel activity during days 2–5. Results are shown as mean ± s.e.m. with individual data points. $^{*}P < 0.05$ in two-sided unpaired *t*-tests. *n* = 8 or 12 mice in **e**–**h**. **i**, **j**, 5-HT^{DRN} neuron activity at the naive condition (**i**) or during the ABA period (**j**). Results are shown as mean ± s.e.m. $^{*}P < 0.05$ among different time points in two-sided unpaired *t*-tests (*n* = 6 mice). Data from control mice were the same as reported in Fig. 4b. **k**, Body weight change. Results are shown as individual data lines. **l**, Survival rate. $P = 0.0496$ in log-rank (Mantel–Cox) test. **m**, Left panel: daily food intake of each individual mouse; right panel: daily food intake during days 2–5. Results are shown as mean ± s.e.m. with individual data points. $^{*}P < 0.05$ in two-sided unpaired *t*-tests. **n**, Left panel: daily running wheel activity of each individual mouse; right panel: daily running wheel activity during days 2–5. Results are shown as mean ± s.e.m. with individual data points. $^{*}P < 0.05$ in two-sided unpaired *t*-tests. *n* = 11 or 12 mice in **k**–**n**. Detailed statistics information is in the Source Data file.

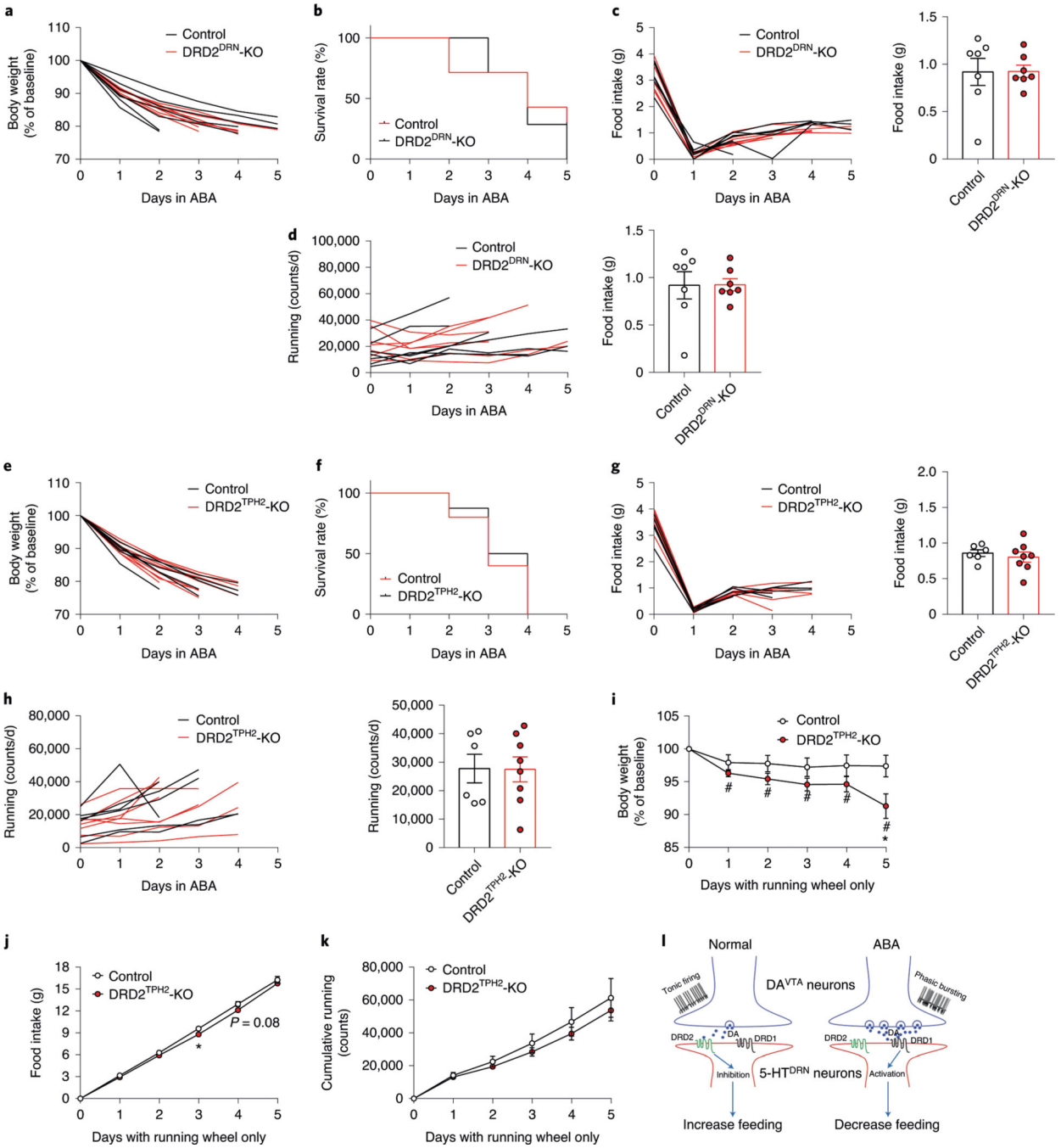

Fig. 6 |. DRD2 prevents anorexia and weight loss during hyperactivity.

a, Body weight change (% of the baseline). Results are shown as individual data lines. Mice were euthanized once they lost more than 20% of body weight. **b**, Survival rate. $P = 0.418$ in log-rank (Mantel–Cox) test. **c**, Left panel: daily food intake of each individual mouse; right panel: daily food intake during days 2–5. Results are shown as mean ± s.e.m. with individual data points. **d**, Left panel: daily running wheel activity of each individual mouse; right panel: daily running wheel activity during days 2–5. Results are shown as mean ± s.e.m. with individual data points. $n = 7$ mice in **a**–**d**. **e**, Body weight change (% of the baseline). Results

are shown as individual data lines. **f**, Survival rate. $P = 0.6977$ in log-rank (Mantel–Cox). **g**, Left panel: daily food intake of each individual mouse; right panel: daily food intake during days 2–5. Results are shown as mean ± s.e.m. with individual data points. **h**, Left panel: daily running wheel activity of each individual mouse; right panel: daily running wheel activity during days 2–5. Results are shown as mean ± s.e.m. with individual data points. $n = 6$ or 8 mice in **e**–**h**. **i**, Body weight change (% of the baseline) during the 5 days exposed to running wheels only. Results are shown as mean ± s.e.m. $*P < 0.05$ between control and $DRD2^{TPH2}$-KO mice during the same period in two-way ANOVA analyses followed by Sidak's post hoc test; $\#P < 0.05$ versus day 0 in $DRD2^{TPH2}$-KO mice in two-way ANOVA analyses followed by Tukey's post hoc test. **j**, Cumulative food intake. Results are shown as mean ± s.e.m. $*P < 0.05$ in two-sided unpaired *t*-tests. **k**, Cumulative running wheel activity. Results are shown as mean ± s.e.m. $n = 6$ or 8 mice in **i**–**k**. **l**, A schematic diagram. Detailed statistics information is in the Source Data file.